Article

Cell Reports

Structures of Gα Proteins in Complex with Their Chaperone Reveal Quality Control Mechanisms

Graphical Abstract

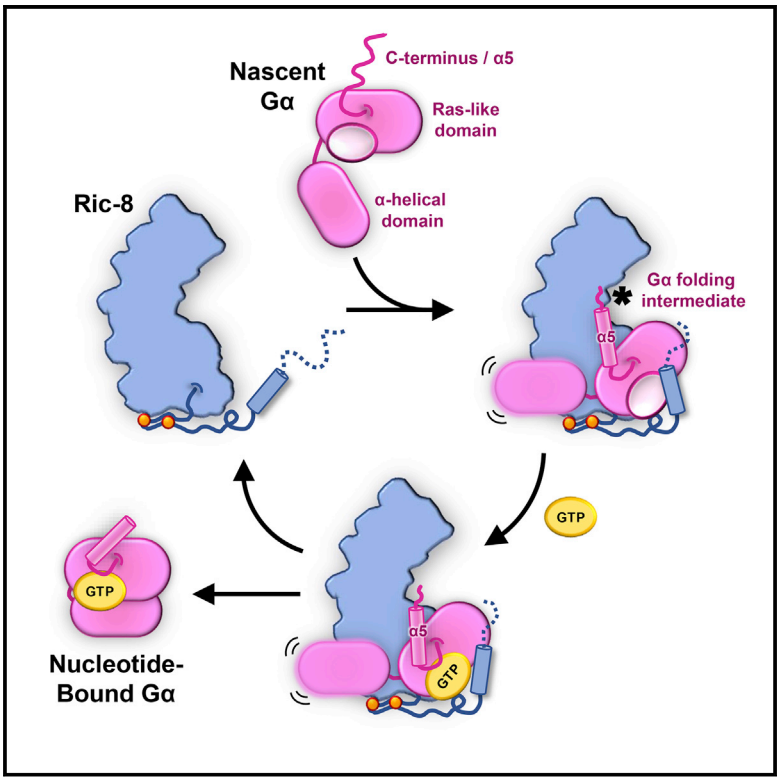

Highlights

- CryoEM structures of $G\alpha_{i1}$ and $G\alpha_{q}$ protein subunits in complex with chaperone Ric-8A
- Ric-8 forms a cradle to accommodate the Ras-like domain of Gα
- Gα C terminus binding to Ric-8 is a prerequisite for GTP-gated Gα release
- Insights into G protein subtype binding specificity by Ric-8 isoforms

Authors

Alpay Burak Seven, Daniel Hilger, Makaía M. Papasergi-Scott, ..., Brian K. Kobilka, Gregory G. Tall, Georgios Skiniotis

Correspondence

daniel.hilger@pharmazie.uni-marburg.de (D.H.),
gregtall@umich.edu (G.G.T.),
yiorgo@stanford.edu (G.S.)

In Brief

Seven et al. present cryoEM structures of Gα subunit folding intermediates in complex with their universal chaperone, Ric-8. Ric-8 forms key interactions with the Ras domain to prepare GTP-gated release of Gα subunits from their chaperone. The structures, complemented by biochemical and cellular experiments, reveal a folding quality control mechanism.

Seven et al., 2020, Cell Reports *30*, 3699–3709
March 17, 2020
https://doi.org/10.1016/j.celrep.2020.02.086

CellPress

Cell Reports
Article

Structures of Gα Proteins in Complex with Their Chaperone Reveal Quality Control Mechanisms

Alpay Burak Seven,[1,2,4] Daniel Hilger,[1,4,*] Makaía M. Papasergi-Scott,[1,2] Li Zhang,[3] Qianhui Qu,[1,2] Brian K. Kobilka,[1] Gregory G. Tall,[3,*] and Georgios Skiniotis[1,2,5,*]
[1]Department of Molecular and Cellular Physiology, Stanford University School of Medicine, Stanford, CA 94305, USA
[2]Department of Structural Biology, Stanford University School of Medicine, Stanford, CA 94305, USA
[3]Department of Pharmacology, University of Michigan Medical School, Ann Arbor, MI 48109, USA
[4]These authors contributed equally
[5]Lead Contact
*Correspondence: daniel.hilger@pharmazie.uni-marburg.de (D.H.), gregtall@umich.edu (G.G.T.), yiorgo@stanford.edu (G.S.)
https://doi.org/10.1016/j.celrep.2020.02.086

SUMMARY

Many chaperones promote nascent polypeptide folding followed by substrate release through ATP-dependent conformational changes. Here we show cryoEM structures of Gα subunit folding intermediates in complex with full-length Ric-8A, a unique chaperone-client system in which substrate release is facilitated by guanine nucleotide binding to the client G protein. The structures of Ric-8A-$G\alpha_i$ and Ric-8A-$G\alpha_q$ complexes reveal that the chaperone employs its extended C-terminal region to cradle the Ras-like domain of Gα, positioning the Ras core in contact with the Ric-8A core while engaging its switch2 nucleotide binding region. The C-terminal α5 helix of Gα is held away from the Ras-like domain through Ric-8A core domain interactions, which critically depend on recognition of the Gα C terminus by the chaperone. The structures, complemented with biochemical and cellular chaperoning data, support a folding quality control mechanism that ensures proper formation of the C-terminal α5 helix before allowing GTP-gated release of Gα from Ric-8A.

INTRODUCTION

Heterotrimeric G proteins, composed of Gα, Gβ, and Gγ subunits, relay the vast majority of intracellular signaling mediated by G protein-coupled receptors (GPCRs), the largest and most diverse class of membrane proteins in eukaryotes. GPCRs respond to a remarkable array of extracellular stimulants, including light, ions, hormones, odorants, neurotransmitters, and natural chemicals, and in turn couple primarily to G proteins to facilitate the exchange of GDP for GTP on the Gα subunit (Hilger et al., 2018). Nucleotide exchange promotes the functional dissociation of Gα-GTP from the Gβγ obligate dimer, leading to downstream signaling through binding to effectors such as adenylyl cyclase, phospholipase C, and ion channels. G proteins are classified based on sequence homology of the Gα subunit into four main sub-classes: $G\alpha_{i/o}$, $G\alpha_{q/11}$, $G\alpha_{s/olf}$, and $G\alpha_{12/13}$, each comprised of multiple isoforms (Wilkie et al., 1992). Accordingly, GPCRs display distinct selectivity profiles for heterotrimeric G proteins, thereby orchestrating precise cellular pathways and signaling outcomes.

The central signaling role of heterotrimeric G proteins, along with their ability to undergo extensive conformational changes during highly tuned receptor coupling and dissociation, has co-evolved with quality control mechanisms for their structural and functional integrity. Recent work has shown that multiple chaperones are necessary for proper folding, assembly, and localization of heterotrimeric G proteins. Chaperonin-containing tailless complex polypeptide-1 (CCT) (Lukov et al., 2005, 2006) and dopamine receptor-interacting protein 78 (DRiP78) (Dupré et al., 2007) were proposed to facilitate the folding of Gβ and Gγ subunits, respectively, while the chaperone phosducin-like protein-1 (PhLP-1) is subsequently involved in the formation of the Gβγ obligate heterodimer (Lukov et al., 2005, 2006). Resistance to inhibitors of cholinesterase-8 (Ric-8) was initially discovered as a gene that positively influenced G protein signaling pathways in a *Caenorhabditis elegans* mutagenesis screen (Miller et al., 1996; Nguyen et al., 1995). Ric-8 proteins are now known to fold nascent Gα subunits prior to G protein heterotrimer formation. The initial *in vitro* work identified Ric-8 as a non-receptor guanine exchange factor (GEF) for Gα proteins (Chan et al., 2011b; Tall et al., 2003), but more recent studies revealed that Ric-8 proteins are molecular chaperones for nascent Gα subunits (Chan et al., 2013; Gabay et al., 2011), thereby explaining the positive influence of their activities on G protein signaling (Papasergi et al., 2015). Besides facilitating Gα folding, the observed Ric-8 GEF activity for Gα subunits (Chan et al., 2011a; Tall et al., 2003; Van Eps et al., 2015) has raised the possibility that these chaperones may also be involved in alternative modes of Gα subunit activation or reamplification of GPCR signaling.

Ric-8 proteins are evolutionarily conserved from fungi to humans (Li et al., 2010; Miller et al., 2000; Papasergi et al., 2015; Wright et al., 2011), although no homologs have been reported in plants and baker's yeast. However, Arr4/Get3 proteins in yeast, structurally unrelated to Ric-8, are shown to be important for the biogenesis and signaling of Gα subunits and act as

non-receptor GEFs (Lee and Dohlman, 2008). There are two isoforms of Ric-8 identified in vertebrates: Ric-8A, which acts within the biosynthetic pathway of the $G\alpha_{i/o}$, $G\alpha_{q/11}$, and $G\alpha_{12/13}$ subclasses, and Ric-8B, which primarily acts on the $G\alpha_{s/olf}$ subfamily (Chan et al., 2013; Gabay et al., 2011; Nagai et al., 2010). The isotypes $G\alpha_{q/11}$, $G\alpha_{12/13}$, and $G\alpha_{olf}$ appear to have the most stringent requirements for Ric-8 in order to be correctly folded and trafficked to the plasma membrane (Chan et al., 2011a; Gabay et al., 2011). Recent crystal structures of a truncated form of Ric-8A alone or in complex with a peptidomimetic of the C-terminal α5 helix of the G protein transducin (G_t) showed that the chaperone is composed of a combination of armadillo (ARM) and Huntington, Elongation Factor 3, PR65/A, TOR1 (HEAT) repeats. The ARM/HEAT repeats form a crescent-shaped core domain, with its concave surface engaging the α5 helix peptidomimetic (Srivastava et al., 2019; Zeng et al., 2019). However, the lack of structural information on full-length Ric-8-Gα complexes has hindered our understanding of the chaperone activity and the mechanism of Gα release from Ric-8, which presumably takes place upon successful Gα folding. Part of the challenge in attaining high-resolution information on folding intermediates is the intrinsic difficulties in obtaining stable complexes that are suitable for structural studies. In general, reported crystal structures of chaperone-client complexes lack high-resolution features of the client protein, thereby limiting the characterization of chaperoning mechanisms at large.

To delineate the critical structural components of the chaperoning and GEF activity of Ric-8 toward Gα protein subunits, we sought to visualize these complexes by cryoEM. To this end, we purified or reconstituted native folding intermediates of two Gα subunits, $G\alpha_q$ and $G\alpha_{i1}$, in complex with Ric-8A in the absence of guanine nucleotides. CryoEM maps of Ric-8A-$G\alpha_q$ and Ric-8A-$G\alpha_{i1}$ at near-atomic resolution provide views of a unique chaperone-client complex and illustrate a striking chaperone mechanism that is employed by Ric-8A to stabilize critical elements for guanine nucleotide coordination by Gα. Mutagenesis coupled to both nucleotide exchange assays and a cellular chaperoning readout indicates that the recognition of the most C-terminal residue of Gα by Ric-8 provides a critical checkpoint for GTP binding to the G protein subunit and its subsequent release from the chaperone. Collectively, these results suggest a quality control mechanism underlying the chaperone and GEF activity of Ric-8 on Gα subunits.

RESULTS

CryoEM Structures of Ric-8A in Complex with $G\alpha_{i1}$ and $G\alpha_q$

For our studies, we employed wild-type full-length $G\alpha_q$ or $G\alpha_{i1}$ proteins and full-length Ric-8A, including its potentially unstructured regions, such as the Ric-8A C-terminal tail, which is required for chaperone activity (Oner et al., 2013; Papasergi-Scott et al., 2018; Thomas et al., 2011). We chose to study these complexes without any stabilizing agent such as antibody fragments or crosslinkers, aiming to preserve both the native structure as well as the conformational flexibility between the chaperone and the client Gα subunit. It has been previously shown that site-specific phosphorylation of Ric-8A is critical for both its chaperone and GEF activity (Papasergi-Scott et al., 2018). To achieve these post-translational modifications, we utilized a baculovirus system to express Ric-8A in insect cells, a strategy that has been shown to produce largely phosphorylated chaperone at positions S435, T440, S522, S523, and S527 (Papasergi-Scott et al., 2018). In the case of Ric-8A-$G\alpha_{i1}$, a complex stable enough for cryoEM imaging was generated by *in vitro* reconstitution from purified Ric-8A and myristoylated $G\alpha_{i1}$ proteins, recombinantly expressed in insect cells and *E. coli*, respectively (Figure S1). Apyrase was added to hydrolyze the GDP released from $G\alpha_{i1}$ upon forming a complex with Ric-8A in order to promote formation of a stable nucleotide-free complex. Due to the lower expression level and protein quality of $G\alpha_q$ compared to $G\alpha_{i1}$ in the absence of chaperone and G$\beta\gamma$, we isolated the Ric-8A-$G\alpha_q$ complex after co-expression of Ric-8A and Gα protein in insect cells. The complex was purified by utilizing an N-terminal GST tag on Ric-8A that was subsequently cleaved by TEV protease treatment. Prior to GST protein purification, apyrase was added to the lysed insect cell suspension for maximal stabilization of the Ric-8A-$G\alpha_q$ complex by hydrolyzing free guanine nucleotides. After GST purification and protease cleavage, the Ric-8A-$G\alpha_q$ complex was further purified by size-exclusion chromatography in order to separate it from free Ric-8A and GST protein. Both purification strategies resulted in stable complexes that were monodisperse as assessed by size-exclusion chromatography and negative stain EM visualization (Figure S1). From these samples, we obtained cryoEM maps of Ric-8A-$G\alpha_q$ and Ric-8A-$G\alpha_{i1}$ with a global indicated resolution of 3.5 Å and 4.1 Å, respectively (Figure 1; Figures S1–S3, S4A, S4B, and Table S1). The structured portion of these assemblies is only ~65 kDa, reinforcing the feasibility of conventional cryoEM for challenging proteins or complexes in the range of 50–100 kDa. These cryoEM maps enabled the modeling of Ric-8A between residues 1–482 in the Ric-8A-$G\alpha_{i1}$ complex and residues 1–451 in the Ric-8A-$G\alpha_q$ complex, while the backbone of the C-terminal region (458–484) was traced with poly-alanine due to the poorer quality of the Ric-8A-$G\alpha_q$ map in the region 451–458. Nevertheless, both models included a relatively long stretch of the C-terminal region of Ric-8A (up to residue 482 or 484), which was not observed previously. The majority of the Ras-like domain residues of both $G\alpha_{i1}$ (residues 32–54 and 193–354) and $G\alpha_q$ (residues 217–359) were also unambiguously modeled in these maps. Although the nucleotide binding regions of Gα are mostly ordered, we do not observe any density for a guanine nucleotide, consistent with the purification of both complexes in the presence of the nucleotide-hydrolyzing enzyme Apyrase and the known stability of Ric-8-Gα nucleotide-free complex. The absence of nucleotide destabilizes the closed conformation of Gα in which the α-helical domain is packed against the Ras-like domain. Thus, in both Ric-8A-$G\alpha_{i1}$ and Ric-8A-$G\alpha_q$ complexes, the α-helical domain opens up and becomes flexible in relation to the rest of the complex, akin to its behavior in nucleotide-free G proteins in complex with a GPCR (Rasmussen et al., 2011; Van Eps et al., 2015; Westfield et al., 2011). Accordingly, the general region occupied by the α-helical domain was masked out in our high-resolution map refinements for Ric-8A-$G\alpha_{i1}$ and Ric-8A-$G\alpha_q$ complexes. However, in lower resolution unmasked reconstructions during

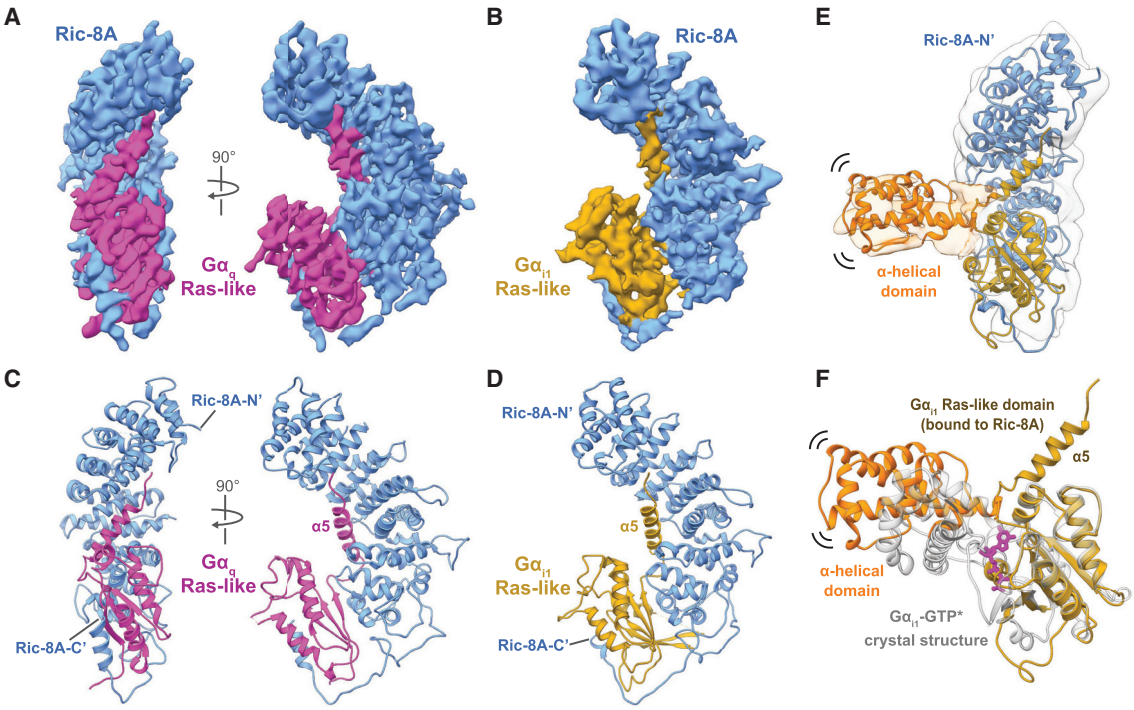

Figure 1. CryoEM Structures of Ric-8A-Gα Complexes

(A and B) Orthogonal views of the cryoEM maps of full-length Ric-8A (blue) bound to (A) full-length $G\alpha_q$ (magenta) at a global resolution of 3.5 Å, or (B) $G\alpha_{i1}$ (gold) at a global resolution of 4.1 Å.

(C and D) Ribbon diagrams of (C) Ric-8A-$G\alpha_q$ and (D) Ric-8A-$G\alpha_{i1}$ models.

(E) A low-resolution map of the Ric-8A-$G\alpha_{i1}$ complex including density for the $G\alpha_{i1}$ α-helical domain that is positioned distal to the Ras-like domain.

(F) Comparison of the $G\alpha_{i1}$-GTPγS crystal structure (gray; PDB: 1GIA) with the Ric-8A-$G\alpha_{i1}$ complex (Ras-like domain: gold, α-helical domain: orange). $G\alpha_{i1}$ adopts a distinct conformation from the canonical GTP-bound state.

initial steps of image processing, we observed partial density for the α-helical domain, jutted away from the nucleotide binding site in an average position that is rotated ~90° compared to the nucleotide-bound structures of $G\alpha_{i1}$ or $G\alpha_q$ (Figures 1E and 1F). Furthermore, the N-terminal helix of both G proteins is not resolved in the Ric-8A complexes, in agreement with its dynamic and unfolded state in the absence of Gβγ, as shown in previous crystal structures and by solution NMR studies of $G\alpha_{i1}$ (Goricanec et al., 2016; Maly and Crowhurst, 2012; Medkova et al., 2002).

The core domain of Ric-8A (residues 1–421), comprised of a combination of nine ARM and HEAT repeats (R1–R9), adopts a crescent-shaped conformation that is similar to the one observed in recent crystal structures of truncated Ric-8A alone (Srivastava et al., 2019; Zeng et al., 2019) (Figure S4C) or in complex with the $G\alpha_t$ α5 helix peptidomimetic (Srivastava et al., 2019) (Figure S4D), with an RMSD of 0.9–1 Å. This observation suggests that the Ric-8A core domain maintains an overall stable conformation in the presence and absence of Gα. Interestingly, however, the core domain of Ric-8A adopts a slightly more compact configuration in its complex with $G\alpha_q$ compared to $G\alpha_{i1}$ (Figure S4B). Furthermore, the bulk of the observable Ric-8A C terminus (residues 421-482) becomes ordered in the presence of $G\alpha_{i1}$ or $G\alpha_q$. This region largely maintains a coil structure, which encapsulates the Ras-like domain of $G\alpha_q$ or $G\alpha_{i1}$, before forming an α-helix most likely comprised of residues 474–484 for $G\alpha_q$ and 474–481 for $G\alpha_{i1}$ (Figure 2). The last C-terminal 40 residues of Ric-8A (490–530), predicted to include a coil/β-strand and an α-helix/coil structure (Figure S4E), have been shown to be critical for the chaperone function of Ric-8A *in vivo*, but are not required for *in vitro* GEF activity (Oner et al., 2013; Papasergi-Scott et al., 2018; Thomas et al., 2011). In our maps, this region appears disordered yet lies within the vicinity of the α-helical domain of Gα, raising the possibility that the 40 C-terminal residues may engage the flexible α-helical domain.

Chaperone-Client Interactions in Ric-8A-Gα Structures

The cryoEM structures of Ric-8A-$G\alpha_{i1}$ and Ric-8A-$G\alpha_q$ reveal three primary interaction surfaces between the chaperone and Gα Ras-like domain (Figure 2A). One interface involves an extensive interaction of the C-terminal α5-helix of Gα with the concave surface of the ARM/HEAT repeats (Figure 2B). A second interface is formed by the β4, β5, and β6 strands of Gα with the R8-R9 ARM/HEAT repeats and a loop formed by residues 453–459 of the extended C terminus of Ric-8A (Figure 2C). The third interface is formed by the C-terminal helix of Ric-8A, which is in contact with switch2, the P loop, and the α3 helix of the Gα Ras-like domain (Figure 2D).

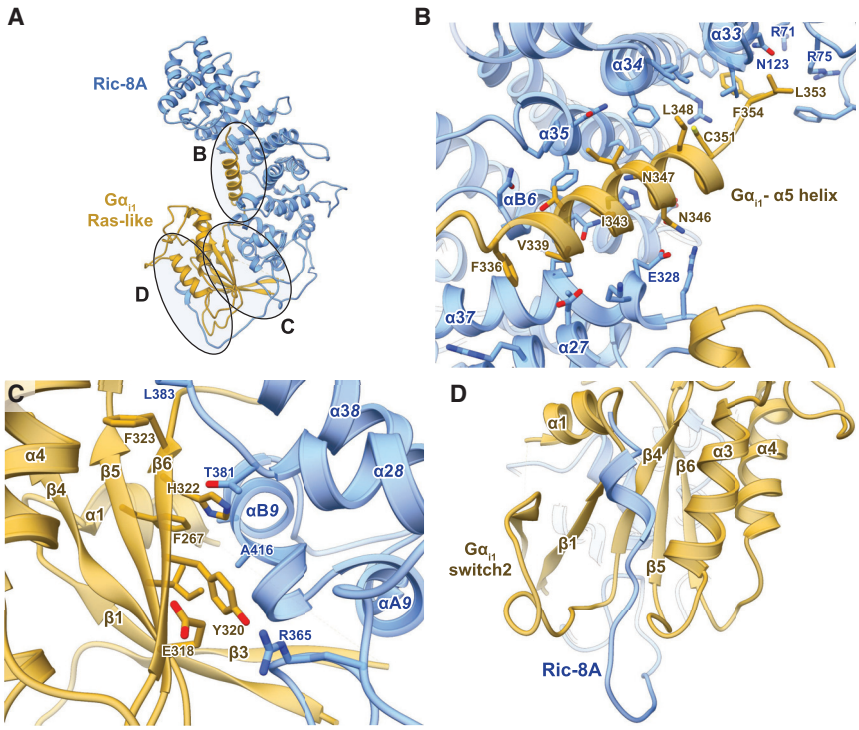

Figure 2. Interfaces in the Ric-8A-Gα_{i1} Complex

(A) Ric-8A binds to Gα through three interfaces.

(B) The α5 helix of Gα_{i1} binds to the concave surface of the Ric-8A N-terminal domain. Within the Ric-8A structure, "α" denotes the α-helical secondary structure followed by the repeat identifier of an individual ARM (1,2, or 3) or HEAT (A or B) helix and ending with the global ARM/HEAT repeat number from the N to C terminus of Ric-8A.

(C) The β5 and β6 strands of Gα_{i1} bind against the last two ARM/HEAT repeats of Ric-8A.

(D) A helical element comprising residues 472–480 of Ric-8A inserts between the switch2 motif and α3 helix of Gα_{i1}.

A comparison of the Gα Ras-like domain conformation in the Ric-8A-Gα maps and nucleotide-bound Gα crystal structures reveals several notable differences. The most distinct difference is the position of the α5 helix and the very C-terminal residues of Gα_{i1} and Gα_q, which interact with the inner concave surface of the ARM/HEAT core domain of Ric-8A. In both complexes, the α5 helix is completely detached from the Ras-like domain and rotated by more than 90° away from its position in the Gα nucleotide-bound conformation (Figures 1E and 1F). The α5 helix is connected to the β6 strand by a loop containing the conserved TCAT motif, a critical element with residues that coordinate the guanine base of GDP or GTP bound to the Ras-like domain. Because of the displacement of the α5 helix (Figure 3A), the TCAT is positioned 3–5 Å away from its nucleotide coordination site (Figure 3B). The positioning of the TCAT motif of Gα_{i1} and Gα_q in complex with Ric-8A is similar to its configuration in nucleotide-free heterotrimeric Gα_{i1}-G$\beta\gamma$ and Gα_{11}-G$\beta\gamma$ (Gα_{11} is a close homolog of Gα_q) proteins in complex with GPCRs (Figures S5A and S5B). Of note, the displacement of the α5 helix from the Ras-like domain core may be promoted by the second helix of the final HEAT repeat (αB9) of Ric-8. Structural alignment of the Ras-like domains shows that the αB9 helix in the Ric-8A-bound Gα_{i1} structure occupies the position of the α5 helix in the GTPγS-bound Gα_{i1} structure (Figures S5C and S5D). Another distinct difference in the Ras-like domain involves the conformation of the switch2 motif and α2 helix that are also important for Gα nucleotide binding. The switch2/α2 elements are mostly disordered in the Ric-8A-Gα_{i1} structure, while in the map of the Ric-8A-Gα_{i1} complex, we can trace their density away from their corresponding conformations in the Gα GTP-bound state (Figures 3A and 3B). This positioning is induced by a C-terminal helix of Ric-8A (474–484), which is sandwiched between the switch2 motif and α3 helix, potentially forming interactions with the P loop and α2 and α3 helices.

The switch1 motif of Gα appears disordered in both of our Ric-8A complex structures, potentially due to the conformational flexibility of the α-helical domain. Additionally, the β2 and β3 strands together with α1 helix of the Ras-like domain are partially ordered in the Ric-8A-Gα_q structure and modestly more ordered in the Ric-8A-Gα_{i1} structure. Notably, the map densities corresponding to these secondary structure elements in both the Gα_{i1} and Gα_q complexes consistently displayed variability across several 3D classes. Although this region is too limited in size to be effectively resolved through particle classification, this observation suggests that the underlying elements are flexible when Gα is engaged with Ric-8A (Figure S3C).

Role of Phosphorylation of Ric-8A-Gα Complexes

The extended C-terminal coil region of Ric-8A includes two patches of phosphorylated residues, one closer to the core ARM/HEAT domain (S435 and T440) and another at the C terminus (S522, S523, and S527) (Figure S4E). Phosphorylation of S435 and T440 are critical for Ric-8A function and highly conserved in both mammalian Ric-8 isoforms (Ric-8A and Ric-8B) and across species (Figure 4D; Figure S6A) (Papasergi-Scott et al., 2018). However, these phosphorylated residues were not represented in the recent crystal structures of Ric-8A (Srivastava et al., 2019; Zeng et al., 2019). In our cryoEM maps, phosphorylated S435 and T440 were both resolved. These critical phosphorylated residues interact with a highly positively charged patch within Ric-8A formed by R345, R348, K349, K352, and R405 (Figure 4). Notably, the phosphate group of S435 in our structures occupies the same position as a reported sulfate ion, which is chemically similar to phosphate, in the crystal structure of truncated Ric-8A alone (Figure S4C) (Zeng et al., 2019). Neither S435 nor T440 residues are directly involved in the interaction between Ric-8A and Gα_{i1}/Gα_q. However, the interaction of the phosphates with the positive patch of Ric-8A anchors an extended coil of Ric-8A closer to the core ARM/HEAT domain. In this conformation, a

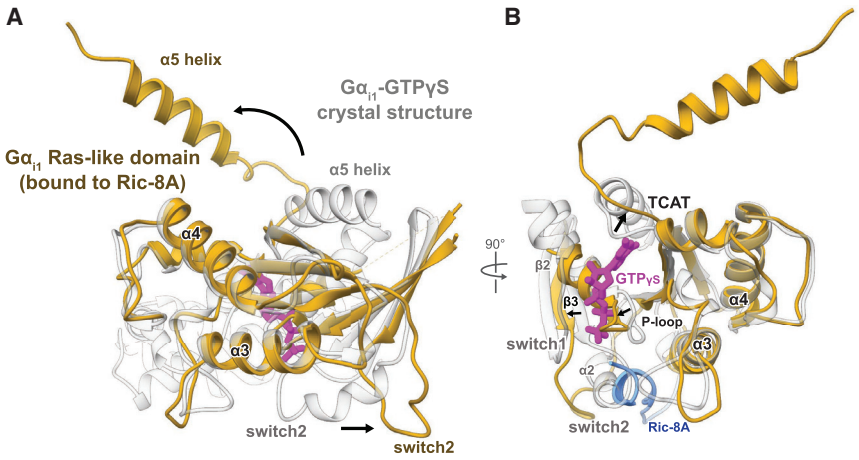

Figure 3. Guanine Nucleotide-free Gα Stabilized by Ric-8A Adopts an Open Conformation

Comparison of the $G\alpha_{i1}$ structures bound to the GTP analog 5′-guanosine-diphosphate-monothiophosphate (GTPγS) (PDB: 1GIA) and to Ric-8A. $G\alpha_{i1}$ adopts a distinct conformation when bound to Ric-8A (gold) from that of the canonical GTP bound state (white).

(A) The α5 helix in the Ric-8A-$G\alpha_{i1}$ complex is rotated more than 90° away from its position in the $G\alpha_{i1}$-GTPγS crystal structure. The Gα switch2 motif is displaced outward compared to its conformation in the Gα-GTPγS structure. The helical segment of Ric-8A interacting with switch2 and the α3 helix of Gα is colored blue, and the rest of Ric-8A was omitted for clarity.

(B) The β6-α5 loop containing the TCAT motif is displaced 3–5 Å outward from its position for guanine nucleotide coordination (thick arrow), and the interface between the α-helical and Ras-like domain is disordered together with the α2 helix and β2 strand.

loop formed by Ric-8A residues 451–461 packs against the Ric-8A core domain itself, which interacts with the Gα Ras-like domain to stabilize the interaction between the Gα β4, β5, and β6 strands with the R8-R9 ARM/HEAT repeats. The effect of T440 phosphorylation was shown to be much more pronounced than S435, presumably because it further stabilizes the coil region in closer proximity to the core, enhancing both the GEF and chaperone activity of Ric-8A (Papasergi-Scott et al., 2018). The interaction of the phosphorylated residues with the positively charged patch of Ric-8A also increases its overall thermal stability in the absence of Gα (Figure S6B), suggesting that it promotes a more compact and stable protein conformation.

Gα Subtype Selectivity by Ric-8A and Ric-8B

To construct a framework for understanding the molecular underpinnings of the G protein isotype specificity of Ric-8A, we analyzed the intermolecular contacts of the Ric-8A-$G\alpha_{i1}$ and the Ric-8A-$G\alpha_q$ structures. Our analysis reveals that the majority of contact residues at the primary interfaces between Ric-8A and the two G protein isotypes are well conserved. This includes the interface between the C-terminal α5 helices of $G\alpha_{i1}$ and $G\alpha_q$ and the concave surface of Ric-8A. In this region, a number of highly conserved hydrophobic residues (L353, L348, I343, V339, and F336; residue numbering based on $G\alpha_{i1}$) mediate conserved hydrophobic and side-chain packing interactions with Ric-8A (Figure 5; Figure S7). The coupling of Ric-8A to $G\alpha_{i1}$ and $G\alpha_q$ is further promoted by key polar interactions that include an H-bond between N347 in $G\alpha_{i1}$ (N352 in $G\alpha_q$) and H273 in Ric-8A and contacts between the last C-terminal carboxyl group of the G protein (F354 and V359 in $G\alpha_{i1}$ and $G\alpha_q$, respectively) and Ric-8A residues R71, R75, and N123 (Figure 5; Figure S7). Even though the last C-terminal residue is not conserved between the two G protein isotypes, the common apolar and polar contacts, described above, similarly position the α5 helices within the concave surface of Ric-8A.

Despite the overall similarity of the interfaces between $G\alpha_{i1}$ or $G\alpha_q$ and Ric-8A, there are a few different contact residues in the α5 helix of the two G protein isotypes. Notably, these variations are well accommodated by Ric-8A through reorientation of side chains, the formation of alternative backbone or side-chain interactions, and conformational changes to adjust the size of the binding grove within the concave surface of the protein. Collectively, these variations result in a larger contact surface between the last 23 C-terminal residues of $G\alpha_q$ and Ric-8A (2,780 $Å^2$) compared to the Ric-8A-$G\alpha_{i1}$ structure (2,201 $Å^2$). In contrast to $G\alpha_q$, $G\alpha_{i1}$ can be folded efficiently when expressed in bacteria that do not have a Ric-8 homolog (Linder et al., 1990). Thus, the tighter interaction between Ric-8A and $G\alpha_q$, in comparison to $G\alpha_{i1}$, might provide an explanation for the strict dependency of Ric-8A for $G\alpha_q$ folding and the lesser dependence of $G\alpha_{i1}$. Furthermore, the larger contact surface may be a reason for the slightly more compact conformation of the chaperone in the Ric-8A-$G\alpha_q$ complex than in the Ric-8A-$G\alpha_{i1}$ structure (Figure S4B). This suggests that Ric-8A is able to adjust the size of its G protein binding groove to accommodate the α5 helices of different G protein isotypes of the $G_{i/o}$, $G_{q/11}$, and $G_{12/13}$ subfamilies, providing an explanation for the observed range of dependencies of various Gα subtypes for Ric-8 in cells.

In addition, we generated a homology model of the Ric-8B-$G\alpha_s$ complex and compared it with the Ric-8A complex structures to better understand G protein selectivity between the two Ric-8 subtypes. This comparison shows that important interactions are shared between the G protein complexes formed by the two Ric-8 subtypes. We observe significant similarities in side-chain interactions within the Ric-8A-$G\alpha_q$ and Ric-8B-$G\alpha_s$ complexes, which might explain the previously observed modest binding of $G\alpha_q$ to Ric-8B (Chan et al., 2011a). However, Ric-8A shows no GEF or chaperone activity for $G\alpha_s$, suggesting that the sequence variations in the α5 helices of $G\alpha_{i1}$, $G\alpha_q$, and $G\alpha_s$ must contribute to the G protein selectivity of the two Ric-8 subtypes. Indeed, superposition of the Ric-8B-$G\alpha_s$ model and Ric-8A-Gα complex structures shows that differences in the amino acid composition of the α5 helix of $G\alpha_s$ are not compatible with the formation of key interactions with Ric-8A (Figure 5; Figure S7). Furthermore, side chain variations in $G\alpha_s$ presumably create some clashes and repulsions that might prevent binding to Ric-8A. Compared to the Ric-8A-Gα structures, the most pronounced difference in the predicted Ric-8B-$G\alpha_s$

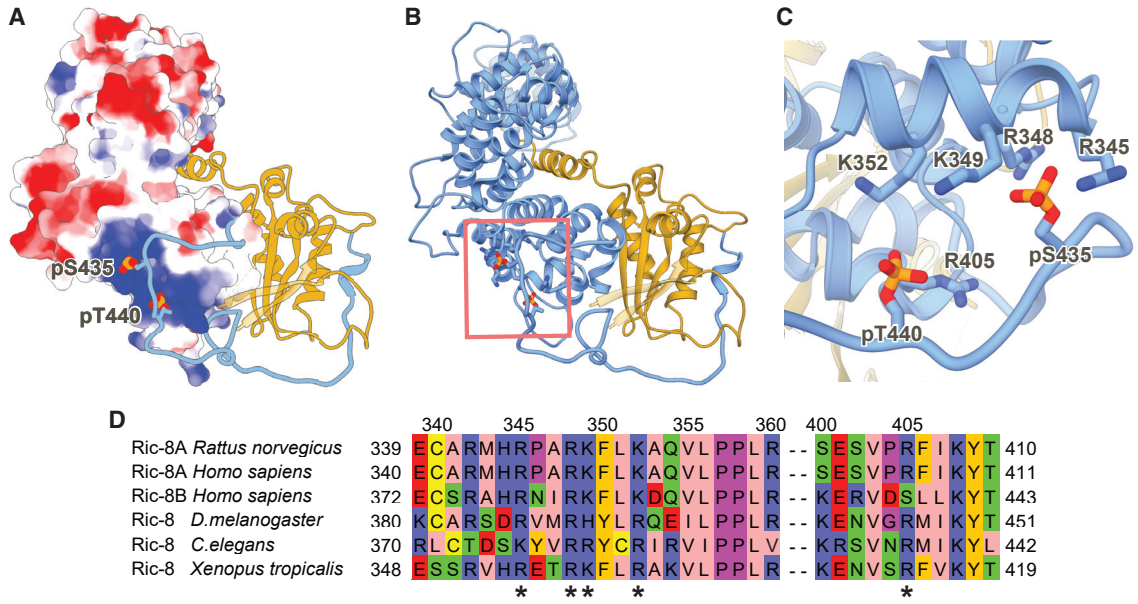

Figure 4. Ric-8A Phosphorylated Residues S435 and T440 Stabilize the R8-R9 ARM/HEAT Interaction with the Ras-like Domain Core

(A) Electrostatic surface representation of Ric-8A 1–421 (−8 to +8 kT/e^{-} electrostatic potential is colored from red to blue respectively). Ric-8A residues 422–482 and Gα_{i1} are shown as ribbon models in blue and gold, respectively. Phosphorylated residues S435 and T440 are shown as spheres.

(B) Ribbon diagram of Ric-8A 1–482 (blue) and Gα_{i1} (gold) of the phosphorylated, full-length Ric-8A-Gα_{i1} complex. Phosphorylated residues S435 and T440 are shown as sticks.

(C) Phosphorylated residues S435 and T440 bind to conserved positively charged residues of Ric-8A.

(D) Sequence alignment of Ric-8 residues interacting with the phosphorylated S435 and T440 sites. The positively charged interacting residues (*) are highly conserved in both mammalian Ric-8 isoforms and across species.

complex is a swap of the side chains of N347 (Gα_{i1}) and H273 (Ric-8A). In Gα_s, N347, which is highly conserved in G proteins that bind to Ric-8A, is replaced by a histidine (H387). This alteration in Gα_s would prevent the formation of the critical polar contact with H273 in Ric-8A and would create a clash between the two side chains (Figure 5D). In contrast, Ric-8B contains an asparagine (N280) at the corresponding position to H273 in Ric-8A that may enable a polar interaction with H387 of Gα_s. An additional steric clash between Ric-8A and the α5 helix of Gα_s might be caused between the glutamine residue Q384 of Gα_s and F232 of Ric-8A. Ric-8B, on the other hand, possesses a smaller side chain (V239) at the homologous position, which is more compatible with Gα_s binding (Figures 5C and 5D). Thus, subtype specificity of Ric-8 for G protein isotypes is not only encoded by the sequences of the α5 helices of the G proteins, as previously proposed (Srivastava et al., 2019), but is also mediated by differences in the G protein binding residues of Ric-8 subtypes that are crucial for the formation of specific contacts with different G protein isotypes (Figure 5; Figure S7).

Ric-8A Maintains Gα_{i1} and Gα_q in a Quasi-folded State Primed for GTP Binding

The cryoEM structures of Ric-8A-Gα_{i1} and Ric-8A-Gα_q reveal that the Gα subunit is partially folded, with key elements required for guanine nucleotide binding positioned with subtle differences in comparison to guanine nucleotide-bound conformations. The ARM/HEAT repeats and the C-terminal helix of Ric-8A interact with the α5 helix and the switch2 motif of Gα, respectively, to position the TCAT motif, the P loop, and switch2 in relatively close proximity to their guanine nucleotide-coordinated conformation, while the extended loop region of Ric-8A wraps around and stabilizes the Ras-like domain of Gα against the chaperone's core. These structural features suggest that the observed Ric-8-bound Gα conformations are primed to engage GTP, which would lead to its release from the chaperone, as it has been shown biochemically (Chan et al., 2011a; Johnston et al., 2008; Tall et al., 2003). By chaperoning critical regions for nucleotide binding, such as the switch2 motif and the α-helix/TCAT-motif module of Gα, Ric-8 presumably ensures proper formation and positioning of the nucleotide binding elements before GTP binding and dissociation of the G protein subunit Gα from Ric-8. The initial guanine nucleotide binding may be facilitated through P loop interactions with the nucleotide phosphates; the three phosphates of GTP can form stronger interactions than the two phosphates of GDP, which could also explain the GTP preference for Gα release. Of note, GTP has a concentration that is 10-fold higher than GDP inside the cell (Traut, 1994), thereby potentially driving the chaperone activity of Ric-8 to evolve as a GTP-gated folding machine. Importantly, displacement of Gα switch2 also protects Gα from premature engagement of the G$\beta\gamma$ heterodimer. Alignment of the Ras-like domain in the structures of the Ric-8A-Gα_{i1} complex and the G$_{i1}$ protein heterotrimer reveals that switch2 is not adopting its partially α-helical conformation in the region that interacts with the Gβ subunit (Figure S5E). Thus, the placement of the Ric-8A C-terminal region

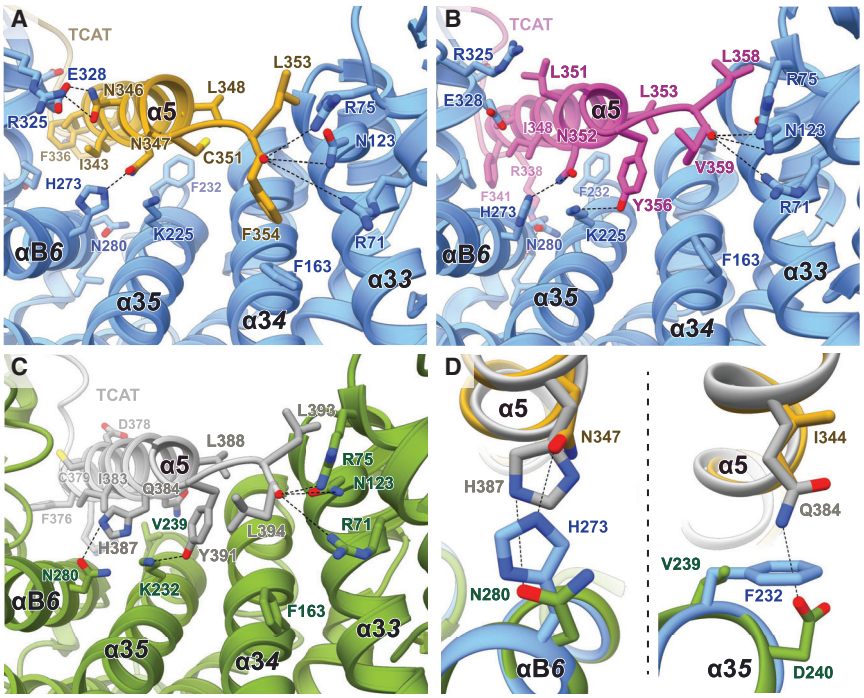

Figure 5. Comparison of the Interactions between Ric-8 and the Gα α5 Helices

(A–C) CryoEM structures of (A) Ric-8A-Gα_{i1} (blue and yellow), (B) Ric-8A-Gα_q (blue and magenta), and (C) the computational model of Ric-8B-Gα_s (green and gray).

(D) Overlay of the side chains from the models Ric-8A-Gα_{i1} and Ric-8B-Gα_s models that are potentially important for Ric-8 specificity.

prepares Ras-like domain elements for GTP binding while prohibiting premature Gβγ engagement (Tall et al., 2003).

Considering these observations, one emerging question is what the trigger is for GTP-gated Gα release from Ric-8A. To further probe this question and delineate the mechanism of chaperone and GEF activity of Ric-8A, we tested the role of key Ric-8 regions observed in our structures for effect on Gα_{i1} stimulated GDP release Gα_{i1} (Figure 6A). In our assays, intrinsic Gα_{i1} GDP release was enhanced by phosphorylated full-length Ric-8A. A Ric-8A truncation that includes the Ric-8A C-terminal region but lacks the entire core domain (MBP-Ric-8A 423–530) stabilized the GDP-bound state of Gα_{i1}, suggesting that the C-terminal extended loop of Ric-8A can interact with Gα switch2, and potentially the alpha helical domain, without requiring an interaction between its ARM/HEAT repeats and the α5 helix of the Gα subunit. Assuming that the α5 helix maintains the same position as observed in the Gα_{i1}-GDP crystal structure (Coleman and Sprang, 1998), this observation suggests that proper TCAT motif coordination with nucleotide stabilizes bound GDP even without proper switch2 motif positioning. In support of this interpretation, the switch2 region of Ras-like domain is not ordered in GDP-bound Gα_{i1} crystal structures (Raw et al., 1997; Rensland et al., 1995; Wittinghofer and Vetter, 2011). Strikingly, we observe that phosphorylated full-length Ric-8A promotes a comparable stabilization of the GDP bound state of Gα_{i1} that lacks only the C-terminal residue F354 (Gα_i-ΔF354), even though this mutant G protein possesses a similar intrinsic GDP release rate as wild-type Gα_{i1}. The importance of the C-terminal residue of Gα_{i1} (F354) is indicated from our structures and the previously reported structure of Ric-8A with the C-terminal Gα transducin α5 helix peptidomimetic (Srivastava et al., 2019). Ric-8A makes several interactions with the C-terminal residues of Gα_{i1} and Gα_q including the coordination of the C-terminal carboxyl group by Ric-8A R71, R75, and N123 and an additional π-π interaction with F163, as described above.

To test the importance of individual residues of Ric-8A that interact with Gα, we utilized an established Ric-8A complementation assay in HEK293T cells in which *RIC-8A* was deleted using CRISPR/Cas9 technology (Papasergi-Scott et al., 2018). Devoid of Ric-8A, the cells have greatly diminished Gα_q, Gα_{13}, and Gα_i protein abundance due to misfolding, which can be rescued to native levels by stable expression of functional Ric-8A (Figures 6A and 6B). Using this system, we created stable cell lines expressing Ric-8A mutated at predicted interaction sites identified from our structures. In cells expressing Ric-8A R71E, R75E, or N123A mutants, we observed a phenotype similar to *RIC-8A* knockout cells whereby the Gα_q abundance defect was not rescued (Figures 6B and 6C; Figure S6C). These results indicate that the polar interactions of Ric-8A with the carboxy-terminus of the C-terminal Gα residue is a critical structural element for Ric-8 chaperone and GEF activities. Similarly, mutation of Ric-8A H273, which participates in hydrogen bonding interactions with the α5 helix and is predicted to be critical for Gα subtype selectivity (see above), significantly abrogates the Gα_q abundance rescue. Single Ric-8A point mutations at other positions showed modest effects, with the exception of A420, which resides at the interface of Ric-8A with the β4-β5-β6 interface of the Gα Ras-like domain. Mutating A420 to a bulky tryptophan brings it into a direct clash with Gα F267, explaining its deleterious effect on chaperoning activity.

Our assays reveal that the residues of the Ric-8 chaperone that engage the C-terminal amino acid of the Gα Ras-like domain dramatically affect nucleotide-dependent release of Gα from Ric-8A. This indicates that binding of the C-terminal residue by the chaperone may be prerequisite for proper Gα folding. Moreover, binding of the α5 helix in the conformation observed in our structures positions the TCAT motif within the β6-α5 loop in close proximity to the nucleotide binding site. Of note, a synthesized 20-mer peptide of the α5 helix of Gα_s did not adopt an α-helical structure in solution but a random coil conformation that was not able to bind to the β_2-adrenergic receptor (Boyhus et al., 2018). This suggests that the α5 helix of G proteins might require the hydrophobic core interactions within the Ras-like domain or Ric-8 to form a helical structure. We therefore predict that binding of

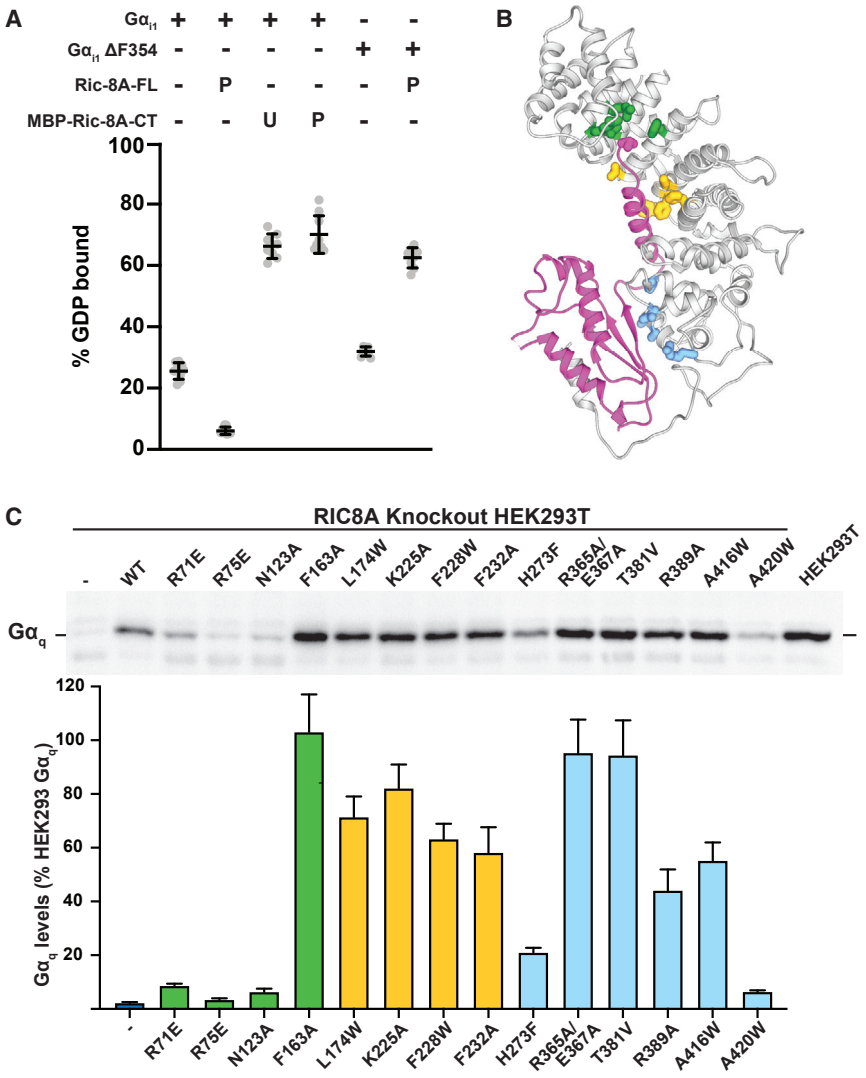

Figure 6. The Chaperone and GEF Activity of Ric-8A Requires Recognition of the Gα C Terminus

(A) Stabilization of the nucleotide-bound state of $G\alpha_{i1}$ by the Ric-8A C terminus and the importance of the α5 helix-Ric-8A interaction for the GEF activity of Ric-8A. The effect of the MBP-fused unphosphorylated "U" or phosphorylated "P" C terminus of Ric-8A (423–530) on Gα GDP release was tested with wild-type $G\alpha_{i1}$ or $G\alpha_{i1}$ Δ354 mutant proteins that were preloaded with ^{3}H-GDP. The amount of bound ^{3}H-GDP after 20 min incubation with or without Ric-8A was determined using a filter binding method and scintillation counting. Error bars are the mean ±SD, n ≥ 3.

(B) Ribbon diagram of the Ric-8A-$G\alpha_q$ complex highlighting putative sites of interaction with the Gα C terminus (green), α5 helix (yellow), or Ras-like domain (blue).

(C) Knockout of *RIC-8A* in HEK293T cells results in a $G\alpha_q$ abundance defect due to Gα misfolding (Papasergi-Scott et al., 2018). The rescue of $G\alpha_q$ abundance upon stable expression of Ric-8A mutants was analyzed by quantitative immunoblotting of cell membrane samples. Representative western blot of membrane-bound $G\alpha_q$ is shown with quantification of $G\alpha_q$ levels as percentage of HEK293T $G\alpha_q$ abundance. Error bars are the mean ± SEM, n = 3.

the nascent α5 helix region and C-terminal residue of Gα to the ARM/HEAT groove of Ric-8A might shield these hydrophobic residues and provide the environment required for folding of this critical region. Furthermore, the chaperoning of the α5 helix away from the Ras core structure would allow the Ras-like domain to fold before it could properly protect the α5 helix. Thus, we propose that engagement of the Gα C terminus by the chaperone serves as both a folding tool for critical regions across the protein and as a quality control check point to release properly folded Gα in response to high-affinity GTP binding.

DISCUSSION

The cryoEM structures of Ric-8A-$G\alpha_{i1}$ and Ric-8A-$G\alpha_q$ complexes along with our *in vitro* and *in vivo* biochemical assays have led us to propose a model for the chaperoning and GEF activity of Ric-8 for Gα subunits (Figure 7). In this model, the C-terminal extended region of Ric-8 may engage the Ras-like domain of a nascent Gα polypeptide, possibly co-translationally, while also protecting it from premature Gβγ heterodimer engagement (Figure S5E). Phosphorylation of the Ric-8 C-terminal region creates interactions that serve to stabilize Gα against the ARM/HEAT repeats, creating a compact chaperoning cradle. In this configuration, the α-helical and Ras-like domain of Gα are kept at a distance to allow their independent folding. The Ras-like domain positioning also allows binding of its C terminus to a distinct position within the Ric-8 core, thereby protecting the amphipathic α5 helix and promoting its folding away from the Ras core domain. The recognition of the C-terminal Gα residue appears to provide a critical proof-reading mechanism that promotes the binding and folding of the α5 helix of Gα within the Ric-8 core. The α5 helix is a key element that undergoes conformational changes to engage a GPCR and to respond to the presence of GTP within the Ras-like domain. Thus, the Ric-8-Gα chaperone-client system has evolved to monitor the integrity of full-length Gα subunit production, with an emphasis on protecting a crucial Gα component. Upon Ric-8-assisted folding, the α5 helix can position the β6-α5 loop containing the TCAT motif in close proximity to engage GTP. Hence, when all nucleotide binding elements are properly folded and positioned, the coordinated engagement of GTP will pull the α5 helix away from the Ric-8 core and instead place it in its properly folded position where it is protected against the Ras-like domain. This compact, canonical configuration of the α5/Ras-like domain in the GTP-bound state likely favors Gα dissociation from Ric-8. GPCR-triggered

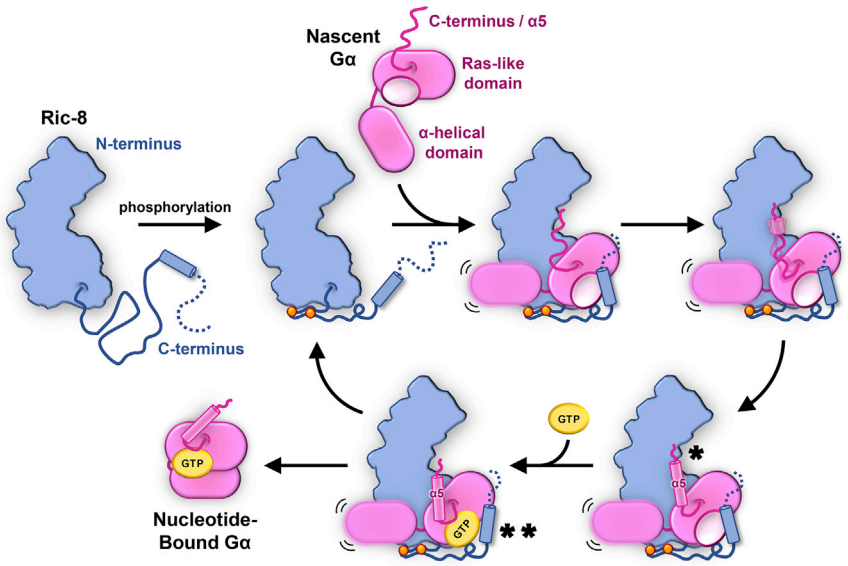

Figure 7. Proposed Mechanism for Ric-8A Chaperoning of Gα

Dual phosphorylation of Ric-8 within a conserved acidic region (orange spheres) facilitates an intramolecular interaction that results in optimal positioning for Gα Ras-like domain engagement by Ric-8. Nascent, nucleotide-free Gα binds Ric-8 either co-translationally or shortly following release from the ribosome. Key interactions occur between the concave surface of the Ric-8 core and the α5-helix of Gα (*) and between a C-terminal helix of Ric-8 with Gα switch2 (**). The recognition of the final C-terminal residue of Gα by Ric-8 serves as a prerequisite for α5-helix folding (*) and positioning of the β6-α5 loop (TCAT motif) to engage GTP (**), thereby releasing properly folded Gα and freeing Ric-8 for subsequent rounds of chaperoning.

guanine nucleotide exchange of Gα subunits within heterotrimeric G proteins is mainly carried out by perturbation of the β1-P loop region, a conformational change of the α5 helix and the associated displacement of the TCAT motif of Gα. Strikingly, Ric-8A uses a very similar strategy to stabilize the nucleotide-free form of Gα, where Ric-8A interacts with the β1 strand and the α5 helix of Gα, which orients the TCAT motif slightly outward from its nucleotide-bound conformation. Furthermore, in the Ric-8A-Gα complex, the α-helical domain is completely detached from the Ras-like domain, similarly to the Gα conformations observed in GPCR-G protein complexes. On the other hand, these domains are closed together in both the GDP- and GTP-bound conformations with the guanine nucleotide packed in between. Unlike GPCRs, Ric-8A additionally interacts with Gα switch2, which is critical for Gβγ binding to Gα. Considering these tailored interactions, together with the fact that, to date, Gα subunits are the only known folding clients for Ric-8, it emerges that Ric-8 is a uniquely evolved chaperone system for the biogenesis of Gα subunits.

Notably, the chaperoning activity of Ric-8 has parallels to other well-described chaperone systems, including the ubiquitous HSP70 foldase. In both cases, upon successful folding of client protein, a nucleotide switch is employed to release the folded client from the chaperone (Figure 7) (Bukau and Horwich, 1998; Mayer and Bukau, 2005). In the case of the HSP70 system, HSP40 nucleotide exchange factors facilitate exchange of ATP for ADP on HSP70 in order to alter the conformation of HSP70 to favor client protein dissociation (Bukau and Horwich, 1998; Mayer and Bukau, 2005). By contrast, Ric-8 proteins are not ATPases, are not known to directly consume cellular energy during Gα subunit folding, and do not use an ADP-ATP switch to release folded Gα. Rather, the nucleotide switch feature is provided by the Gα client protein itself, which likely serves as the final checkpoint for the production of properly folded G protein. As a molecular chaperone, Ric-8A cradles the majority of the Gα Ras-like domain to facilitate its proper folding and development of the Gα guanine nucleotide binding pocket (Figures 1 and 7).

When Gα is capable to competently bind GTP (i.e., is folded) it switches to its active conformation that has low affinity for Ric-8 and the complex dissociates (Figure 7). An appealing future direction of our work is to examine the prospect that Ric-8 may serve as a co-translational Gα subunit chaperone. The finding that the extreme C-terminal residue of Gα is required for folded Gα release from Ric-8 provides a timing or checkpoint mechanism during translation to ensure that the Ras-like domain core is properly folded prior to productive GTP binding and release. A lesser known fact of various isotypes of Gα subunits purified from bacteria or without the presence of Ric-8 is that a substantial portion of the protein preparations exist in a soluble, monomeric form that is inactive as far as the ability to bind guanine nucleotide, e.g., $G\alpha_q$. This inactive, soluble form of Gα has been proposed to be a nucleotide-free, alternatively folded bottleneck conformation. The function of Ric-8 may therefore be to disfavor such inactive conformational bottlenecks and provide the chaperone activity to favor folding of active Gα.

STAR★METHODS

Detailed methods are provided in the online version of this paper and include the following:

- KEY RESOURCES TABLE
- LEAD CONTACT AND MATERIALS AVAILABILITY
- EXPERIMENTAL MODEL AND SUBJECT DETAILS
- METHOD DETAILS
  - Expression and purification of myristoylated $G\alpha_{i1}$ for Ric-8A complex formation
  - Formation and purification of the Ric-8A-$G\alpha_{i1}$ complex
  - Expression and purification of the Ric-8A-$G\alpha_q$ complex
  - Expression and purification of non-myristoylated $G\alpha_{i1}$ protein and the $G\alpha_{i1}$-ΔF354 mutant
  - Purification of His8-MBP-Ric-8A(423-530) for GDP release assay
  - *In vitro* phosphorylation of MBP-Ric-8A (423-530)

- GDP release assay
- Fluorescence polarization spectroscopy
- CryoEM data acquisition and processing
- Model building and refinement
- Generation of a homology model of Ric-8B-Gα_s
- Protein Thermal Stability Assays
- Cell culture and cell line generation
- Membrane preparation and Immunoblotting
- Multiple sequence alignment and secondary structure prediction

● QUANTIFICATION AND STATISTICAL ANALYSIS
● DATA AND CODE AVAILABILITY

SUPPLEMENTAL INFORMATION

Supplemental Information can be found online at https://doi.org/10.1016/j.celrep.2020.02.086.

ACKNOWLEDGMENTS

We would like to thank Matthieu Masureel for fluorescent polarization assays, Rashed Chowdhury for initial data processing, Gozde Eskici and Michael J. Robertson for fruitful discussions, Elizabeth Ann Montabana and David A. Bushnell for assistance with cryoEM, and Wenxi Yu for technical support. Financial support was provided by the National Institutes of Health (Grants R01 NS092695 to G.S., R01NS028471 to B.K.K., T32-GM06841 and PhRMA Foundation predoctoral fellowship to M.M.P.-S., and GM088242 to G.G.T.)

AUTHOR CONTRIBUTIONS

M.M.P.-S., and D.H. purified proteins. Biochemistry assays were performed by D.H., and A.B.S. Cell-based assays were performed by L.Z. under supervision of G.G.T. A.B.S. and Q.Q. obtained cryoEM data, and A.B.S. processed cryoEM data and generated cryoEM maps under supervision of G.S. Modeling was performed by D.H. and A.B.S. under supervision of G.S. A.B.S., D.H., M.M.P.-S., G.G.T., and G.S. wrote the manuscript with input from B.K.K.

DECLARATION OF INTERESTS

B.K.K. is a co-founder of and consultant for ConfometRx, Inc.

Received: December 29, 2019
Revised: January 31, 2020
Accepted: February 24, 2020
Published: March 2, 2020

REFERENCES

Adams, P.D., Afonine, P.V., Bunkóczi, G., Chen, V.B., Echols, N., Headd, J.J., Hung, L.W., Jain, S., Kapral, G.J., Grosse Kunstleve, R.W., et al. (2011). The Phenix software for automated determination of macromolecular structures. Methods *55*, 94–106.

Boyhus, L.-E., Danielsen, M., Bengtson, N.S., Kunze, M.B.A., Kubiak, X., Sminia, T.J., Løper, J.H., Tran, P.T., Lindorff-Larsen, K., Rasmussen, S.G.F., et al. (2018). G_s protein peptidomimetics as allosteric modulators of the beta(2)-adrenergic receptor. RSC Adv. *8*, 2219–2228.

Bukau, B., and Horwich, A.L. (1998). The Hsp70 and Hsp60 chaperone machines. Cell *92*, 351–366.

Chan, P., Gabay, M., Wright, F.A., Kan, W., Oner, S.S., Lanier, S.M., Smrcka, A.V., Blumer, J.B., and Tall, G.G. (2011a). Purification of heterotrimeric G protein alpha subunits by GST-Ric-8 association: primary characterization of purified G alpha(olf). J. Biol. Chem. *286*, 2625–2635.

Chan, P., Gabay, M., Wright, F.A., and Tall, G.G. (2011b). Ric-8B is a GTP-dependent G protein alphas guanine nucleotide exchange factor. J. Biol. Chem. *286*, 19932–19942.

Chan, P., Thomas, C.J., Sprang, S.R., and Tall, G.G. (2013). Molecular chaperoning function of Ric-8 is to fold nascent heterotrimeric G protein α subunits. Proc. Natl. Acad. Sci. USA *110*, 3794–3799.

Coleman, D.E., and Sprang, S.R. (1998). Crystal structures of the G protein Gi alpha 1 complexed with GDP and Mg2+: a crystallographic titration experiment. Biochemistry *37*, 14376–14385.

Dupré, D.J., Robitaille, M., Richer, M., Ethier, N., Mamarbachi, A.M., and Hébert, T.E. (2007). Dopamine receptor-interacting protein 78 acts as a molecular chaperone for Ggamma subunits before assembly with Gbeta. J. Biol. Chem. *282*, 13703–13715.

Emsley, P., Lohkamp, B., Scott, W.G., and Cowtan, K. (2010). Features and development of Coot. Acta Crystallogr. D Biol. Crystallogr. *66*, 486–501.

Flock, T., Ravarani, C.N.J., Sun, D., Venkatakrishnan, A.J., Kayikci, M., Tate, C.G., Veprintsev, D.B., and Babu, M.M. (2015). Universal allosteric mechanism for Gα activation by GPCRs. Nature *524*, 173–179.

Gabay, M., Pinter, M.E., Wright, F.A., Chan, P., Murphy, A.J., Valenzuela, D.M., Yancopoulos, G.D., and Tall, G.G. (2011). Ric-8 proteins are molecular chaperones that direct nascent G protein α subunit membrane association. Sci. Signal. *4*, ra79.

Goricanec, D., Stehle, R., Egloff, P., Grigoriu, S., Plückthun, A., Wagner, G., and Hagn, F. (2016). Conformational dynamics of a G-protein α subunit is tightly regulated by nucleotide binding. Proc. Natl. Acad. Sci. USA *113*, E3629–E3638.

Hilger, D., Masureel, M., and Kobilka, B.K. (2018). Structure and dynamics of GPCR signaling complexes. Nat. Struct. Mol. Biol. *25*, 4–12.

Johnston, C.A., Afshar, K., Snyder, J.T., Tall, G.G., Gönczy, P., Siderovski, D.P., and Willard, F.S. (2008). Structural determinants underlying the temperature-sensitive nature of a Galpha mutant in asymmetric cell division of Caenorhabditis elegans. J. Biol. Chem. *283*, 21550–21558.

Jones, D.T. (1999). Protein secondary structure prediction based on position-specific scoring matrices. J. Mol. Biol. *292*, 195–202.

Lee, M.J., and Dohlman, H.G. (2008). Coactivation of G protein signaling by cell-surface receptors and an intracellular exchange factor. Curr. Biol. *18*, 211–215.

Li, Y., Yan, X., Wang, H., Liang, S., Ma, W.B., Fang, M.Y., Talbot, N.J., and Wang, Z.Y. (2010). MoRic8 Is a novel component of G-protein signaling during plant infection by the rice blast fungus Magnaporthe oryzae. Mol. Plant Microbe Interact. *23*, 317–331.

Liebschner, D., Afonine, P.V., Baker, M.L., Bunkóczi, G., Chen, V.B., Croll, T.I., Hintze, B., Hung, L.W., Jain, S., McCoy, A.J., et al. (2019). Macromolecular structure determination using X-rays, neutrons and electrons: recent developments in Phenix. Acta Crystallogr. D Struct. Biol. *75*, 861–877.

Linder, M.E., Ewald, D.A., Miller, R.J., and Gilman, A.G. (1990). Purification and characterization of Go alpha and three types of Gi alpha after expression in Escherichia coli. J. Biol. Chem. *265*, 8243–8251.

Lukov, G.L., Hu, T., McLaughlin, J.N., Hamm, H.E., and Willardson, B.M. (2005). Phosducin-like protein acts as a molecular chaperone for G protein betagamma dimer assembly. EMBO J. *24*, 1965–1975.

Lukov, G.L., Baker, C.M., Ludtke, P.J., Hu, T., Carter, M.D., Hackett, R.A., Thulin, C.D., and Willardson, B.M. (2006). Mechanism of assembly of G protein betagamma subunits by protein kinase CK2-phosphorylated phosducin-like protein and the cytosolic chaperonin complex. J. Biol. Chem. *281*, 22261–22274.

Madeira, F., Park, Y.M., Lee, J., Buso, N., Gur, T., Madhusoodanan, N., Basutkar, P., Tivey, A.R.N., Potter, S.C., Finn, R.D., and Lopez, R. (2019). The EMBL-EBI search and sequence analysis tools APIs in 2019. Nucleic Acids Res. *47* (*W1*), W636–W641.

Maly, J., and Crowhurst, K.A. (2012). Expression, purification and preliminary NMR characterization of isotopically labeled wild-type human heterotrimeric G protein αi1. Protein Expr. Purif. *84*, 255–264.

Mastronarde, D.N. (2005). Automated electron microscope tomography using robust prediction of specimen movements. J. Struct. Biol. *152*, 36–51.

Mayer, M.P., and Bukau, B. (2005). Hsp70 chaperones: cellular functions and molecular mechanism. Cell. Mol. Life Sci. *62*, 670–684.

Medkova, M., Preininger, A.M., Yu, N.J., Hubbell, W.L., and Hamm, H.E. (2002). Conformational changes in the amino-terminal helix of the G protein alpha(i1) following dissociation from Gbetagamma subunit and activation. Biochemistry *41*, 9962–9972.

Miller, K.G., Alfonso, A., Nguyen, M., Crowell, J.A., Johnson, C.D., and Rand, J.B. (1996). A genetic selection for Caenorhabditis elegans synaptic transmission mutants. Proc. Natl. Acad. Sci. USA *93*, 12593–12598.

Miller, K.G., Emerson, M.D., McManus, J.R., and Rand, J.B. (2000). RIC-8 (Synembryn): a novel conserved protein that is required for G(q)alpha signaling in the C. elegans nervous system. Neuron *27*, 289–299.

Moerke, N.J. (2009). Fluorescence Polarization (FP) Assays for Monitoring Peptide-Protein or Nucleic Acid-Protein Binding. Curr. Protoc. Chem. Biol. *1*, 1–15.

Mumby, S.M., and Linder, M.E. (1994). Myristoylation of G-protein alpha subunits. Methods Enzymol. *237*, 254–268.

Nagai, Y., Nishimura, A., Tago, K., Mizuno, N., and Itoh, H. (2010). Ric-8B stabilizes the alpha subunit of stimulatory G protein by inhibiting its ubiquitination. J. Biol. Chem. *285*, 11114–11120.

Nguyen, M., Alfonso, A., Johnson, C.D., and Rand, J.B. (1995). Caenorhabditis elegans mutants resistant to inhibitors of acetylcholinesterase. Genetics *140*, 527–535.

Nishimura, A., Kitano, K., Takasaki, J., Taniguchi, M., Mizuno, N., Tago, K., Hakoshima, T., and Itoh, H. (2010). Structural basis for the specific inhibition of heterotrimeric Gq protein by a small molecule. Proc. Natl. Acad. Sci. USA *107*, 13666–13671.

Oner, S.S., Maher, E.M., Gabay, M., Tall, G.G., Blumer, J.B., and Lanier, S.M. (2013). Regulation of the G-protein regulatory-Gα*i* signaling complex by nonreceptor guanine nucleotide exchange factors. J. Biol. Chem. *288*, 3003–3015.

Papasergi, M.M., Patel, B.R., and Tall, G.G. (2015). The G protein α chaperone Ric-8 as a potential therapeutic target. Mol. Pharmacol. *87*, 52–63.

Papasergi-Scott, M.M., Stoveken, H.M., MacConnachie, L., Chan, P.Y., Gabay, M., Wong, D., Freeman, R.S., Beg, A.A., and Tall, G.G. (2018). Dual phosphorylation of Ric-8A enhances its ability to mediate G protein α subunit folding and to stimulate guanine nucleotide exchange. Sci. Signal. *11*, eaap8113. https://doi.org/10.1126/scisignal.aap8113.

Pettersen, E.F., Goddard, T.D., Huang, C.C., Couch, G.S., Greenblatt, D.M., Meng, E.C., and Ferrin, T.E. (2004). UCSF Chimera–a visualization system for exploratory research and analysis. J. Comput. Chem. *25*, 1605–1612.

Punjani, A., Rubinstein, J.L., Fleet, D.J., and Brubaker, M.A. (2017). cryoSPARC: algorithms for rapid unsupervised cryo-EM structure determination. Nat. Methods *14*, 290–296.

Rasmussen, S.G., DeVree, B.T., Zou, Y., Kruse, A.C., Chung, K.Y., Kobilka, T.S., Thian, F.S., Chae, P.S., Pardon, E., Calinski, D., et al. (2011). Crystal structure of the β2 adrenergic receptor-Gs protein complex. Nature *477*, 549–555.

Raw, A.S., Coleman, D.E., Gilman, A.G., and Sprang, S.R. (1997). Structural and biochemical characterization of the GTPgammaS-, GDP.Pi-, and GDP-bound forms of a GTPase-deficient Gly42–> Val mutant of Gialpha1. Biochemistry *36*, 15660–15669.

Rensland, H., John, J., Linke, R., Simon, I., Schlichting, I., Wittinghofer, A., and Goody, R.S. (1995). Substrate and product structural requirements for binding of nucleotides to H-ras p21: the mechanism of discrimination between guanosine and adenosine nucleotides. Biochemistry *34*, 593–599.

Rohou, A., and Grigorieff, N. (2015). CTFFIND4: Fast and accurate defocus estimation from electron micrographs. J. Struct. Biol. *192*, 216–221.

Rossi, A.M., and Taylor, C.W. (2011). Analysis of protein-ligand interactions by fluorescence polarization. Nat. Protoc. *6*, 365–387.

Schaffner, W., and Weissmann, C. (1973). A rapid, sensitive, and specific method for the determination of protein in dilute solution. Anal. Biochem. *56* (*2*), 502–514. https://doi.org/10.1016/0003-2697(73)90217-0.

Srivastava, D., Gakhar, L., and Artemyev, N.O. (2019). Structural underpinnings of Ric8A function as a G-protein α-subunit chaperone and guanine-nucleotide exchange factor. Nat. Commun. *10*, 3084.

Tall, G.G., Krumins, A.M., and Gilman, A.G. (2003). Mammalian Ric-8A (synembryn) is a heterotrimeric Galpha protein guanine nucleotide exchange factor. J. Biol. Chem. *278*, 8356–8362.

Tan, Y.Z., Baldwin, P.R., Davis, J.H., Williamson, J.R., Potter, C.S., Carragher, B., and Lyumkis, D. (2017). Addressing preferred specimen orientation in single-particle cryo-EM through tilting. Nat. Methods *14*, 793–796.

Thomas, C.J., Briknarová, K., Hilmer, J.K., Movahed, N., Bothner, B., Sumida, J.P., Tall, G.G., and Sprang, S.R. (2011). The nucleotide exchange factor Ric-8A is a chaperone for the conformationally dynamic nucleotide-free state of Gα*i*1. PLoS ONE *6*, e23197.

Traut, T.W. (1994). Physiological concentrations of purines and pyrimidines. Mol. Cell. Biochem. *140*, 1–22.

Van Eps, N., Thomas, C.J., Hubbell, W.L., and Sprang, S.R. (2015). The guanine nucleotide exchange factor Ric-8A induces domain separation and Ras domain plasticity in Gα*i*1. Proc. Natl. Acad. Sci. USA *112*, 1404–1409.

Wall, M.A., Coleman, D.E., Lee, E., Iñiguez-Lluhi, J.A., Posner, B.A., Gilman, A.G., and Sprang, S.R. (1995). The structure of the G protein heterotrimer Gi alpha 1 beta 1 gamma 2. Cell *83*, 1047–1058.

Waterhouse, A.M., Procter, J.B., Martin, D.M., Clamp, M., and Barton, G.J. (2009). Jalview Version 2–a multiple sequence alignment editor and analysis workbench. Bioinformatics *25*, 1189–1191.

Waterhouse, A., Bertoni, M., Bienert, S., Studer, G., Tauriello, G., Gumienny, R., Heer, F.T., de Beer, T.A.P., Rempfer, C., Bordoli, L., et al. (2018). SWISS-MODEL: homology modelling of protein structures and complexes. Nucleic Acids Res. *46* (*W1*), W296–W303.

Westfield, G.H., Rasmussen, S.G., Su, M., Dutta, S., DeVree, B.T., Chung, K.Y., Calinski, D., Velez-Ruiz, G., Oleskie, A.N., Pardon, E., et al. (2011). Structural flexibility of the G alpha s alpha-helical domain in the beta2-adrenoceptor Gs complex. Proc. Natl. Acad. Sci. USA *108*, 16086–16091.

Wilkie, T.M., Gilbert, D.J., Olsen, A.S., Chen, X.N., Amatruda, T.T., Korenberg, J.R., Trask, B.J., de Jong, P., Reed, R.R., Simon, M.I., et al. (1992). Evolution of the mammalian G protein alpha subunit multigene family. Nat. Genet. *1*, 85–91.

Williams, C.J., Headd, J.J., Moriarty, N.W., Prisant, M.G., Videau, L.L., Deis, L.N., Verma, V., Keedy, D.A., Hintze, B.J., Chen, V.B., et al. (2018). MolProbity: More and better reference data for improved all-atom structure validation. Protein Sci. *27*, 293–315.

Wittinghofer, A., and Vetter, I.R. (2011). Structure-function relationships of the G domain, a canonical switch motif. Annu. Rev. Biochem. *80*, 943–971.

Wright, S.J., Inchausti, R., Eaton, C.J., Krystofova, S., and Borkovich, K.A. (2011). RIC8 is a guanine-nucleotide exchange factor for Galpha subunits that regulates growth and development in Neurospora crassa. Genetics *189*, 165–176.

Zeng, B., Mou, T.C., Doukov, T.I., Steiner, A., Yu, W., Papasergi-Scott, M., Tall, G.G., Hagn, F., and Sprang, S.R. (2019). Structure, Function, and Dynamics of the Galpha Binding Domain of Ric-8A. Structure *27*, 1137–1147.

Zhang, K. (2016). Gctf: Real-time CTF determination and correction. J. Struct. Biol. *193*, 1–12.

Zheng, S.Q., Palovcak, E., Armache, J.P., Verba, K.A., Cheng, Y., and Agard, D.A. (2017). MotionCor2: anisotropic correction of beam-induced motion for improved cryo-electron microscopy. Nat. Methods *14*, 331–332.

Zivanov, J., Nakane, T., Forsberg, B.O., Kimanius, D., Hagen, W.J., Lindahl, E., and Scheres, S.H. (2018). New tools for automated high-resolution cryo-EM structure determination in RELION-3. eLife *7*, e42166. https://doi.org/10.7554/eLife.42166.

STAR★METHODS

KEY RESOURCES TABLE

REAGENT or RESOURCE	SOURCE	IDENTIFIER
Antibodies		
FLAG M2 antibody	Millipore-Sigma	Cat# F3165; RRID: AB_259529
Gαq/11 antibody	Millipore-Sigma	Cat# G4290; RRID: AB_259903
Bacterial and Virus Strains		
JM109(DE3)	Promega	Cat# P9801
Rosetta 2(DE3)	Sigma	Cat# 71400
DH5α $T1^R$	Invitrogen	12297016
Chemicals, Peptides, and Recombinant Proteins		
Benzamidine	Sigma	Cat# L2884
Leupeptin	Sigma	Cat# L2884
CHAPS	Anatrace	Cat# C316
GDP	Sigma	Cat# 7127
ESF921 culture medium	Expression Systems	Cat# 96-001
TCEP	Sigma	Cat# C4706
[^{3}H]-GDP	PerkinElmer	Cat# NET966250UC
IPTG	Goldbio	Cat# I2481
Myristic acid	Sigma	Cat# M3128
Lysozyme	Sigma	Cat# 62970
Chelating Sepharose Fast Flow	GE Healthcare	Cat# 17057502
DTT	Goldbio	Cat# DTT
Apyrase	NEB	Cat# M0398L
Glutathione Resin	Genscript	Cat# L00206
Casein Kinase II (CKII)	NEB	Cat# P6010L
Guanosine 5′-O-(3-thiotriphosphate) (GTPγS)	Abcam	Cat# ab146662
FITC-labeled Ric-8A (504-530) peptide	Analytical Core Facility, Tufts University	Custom Synthesis
Hygromycin B	Invitrogen	10687010
DMEM	Invitrogen	11995065
FBS, USDA	Invitrogen	10437036
Mixed cellulose membrane	EMD Millipore	Cat# GSWP02500
HiPrep Phenyl HP 16/10	GE Healthcare	Cat# 29018184
SYPRO Orange	Life Technologies Corporation	Cat# S6650
Deposited Data		
Ric-8A-$G\alpha_q$ coordinates	This paper	PDB: 6VU5
Ric-8A-$G\alpha_{i1}$ coordinates	This paper	PDB: 6VU7
Ric-8A-$G\alpha_q$ EM map	This paper	EMDB: EMD-21387
Ric-8A-$G\alpha_{i1}$ EM map	This paper	EMDB: EMD-21388
Experimental Models: Cell Lines		
Trichuplusia ni	Expression Systems	Cat# 94-002S
HEK293T	ATCC	CRL-11268
HEK293T *RIC-8A* knockout	Papasergi-Scott et al.	N/A
Oligonucleotides		
Refer to Table S2		N/A
Recombinant DNA		
pFastbac-$G\alpha_q$	This work	N/A
pFastbac-GST-TEV-Ric-8A	Chan et al., 2011a	N/A

(*Continued on next page*)

Continued

REAGENT or RESOURCE	SOURCE	IDENTIFIER
pMal-His8-MBP-Ric-8A(423-530)	This work	N/A
pETDuet-1-Gα_{i1}(6His between M119 and T120)/ NMT1	This work	N/A
pET21a-His6-3C-Gα_{i1}	This work	N/A
pET21a-His6-3C-Gα_{i1}-ΔF354	This work	N/A
3X-FLAG-Ric-8A pcDNA3.1 Hygro	This work	N/A
Software and Algorithms		
UCSF Chimera	Pettersen et al., 2004	https://www.cgl.ucsf.edu/chimera/
COOT	Emsley et al., 2010	https://www2.mrc-lmb.cam.ac.uk/personal/pemsley/coot/
Molprobity	Williams et al., 2018	http://molprobity.biochem.duke.edu/
Phenix 1.17.1	Liebschner et al., 2019	https://www.phenix-online.org/
Prism 8	GraphPad	https://www.graphpad.com/
SWISS-MODEL	Waterhouse et al., 2018	https://swissmodel.expasy.org/
Adobe Photoshop 2020	Adobe	https://www.adobe.com/
Adobe Illustrator 2020	Adobe	https://www.adobe.com/
Relion3	Zivanov et al., 2018	https://www3.mrc-lmb.cam.ac.uk/relion/index.php?title=Main_Page
SerialEM	Mastronarde, 2005	https://bio3d.colorado.edu/SerialEM/
CtfFind4	Rohou and Grigorieff, 2015	https://grigoriefflab.umassmed.edu/ctffind4
Gctf	Zhang, 2016	https://www.mrc-lmb.cam.ac.uk/kzhang/
MotionCor2	Zheng et al., 2017	https://emcore.ucsf.edu/ucsf-motioncor2
3DFSC	Liebschner et al., 2019	https://3dfsc.salk.edu/
Other		
SYPRO Orange	Life Technologies Corporation	Cat# S6650

LEAD CONTACT AND MATERIALS AVAILABILITY

Further information and requests for resources and reagents should be directed to and will be fulfilled by the Lead Contact, Georgios Skiniotis (yiorgo@stanford.edu).

All the reagents generated in this study will be made available on request but we may require a payment and/or a completed Materials Transfer Agreement if there is potential for commercial application.

EXPERIMENTAL MODEL AND SUBJECT DETAILS

Rat GST-TEV-Ric-8A was expressed in Tni (*Trichoplusia ni*) cells infected with recombinant baculovirus (pFastBac, Invitrogen). Tni cells were obtained from Expression Systems, LLC. Rat GST-TEV-Ric-8A together with human Gα_q were expressed in Tni (*Trichuplusia ni*) cells infected with two recombinant baculoviruses (pFastBac, Invitrogen). Human 6His-3C-Gα_{i1} WT or 6His-3C-Gα_{i1} ΔF354 were expressed in Rosetta 2(DE3) cells (Merck Millipore). Human Gα_{i1} (6His between M119 and T120) was expressed in JM109 (DE3) cells (Promega). MBP-Ric-8A (423-530) was expressed in Rosetta 2 (DE3) cells. The HEK293T cell line (CRL-11268) was obtained from the American Type Culture Collection (ATCC). Crispr/Cas9 procedures were used previously to delete *RIC-8A* in the HEK293T cells (Papasergi-Scott et al., 2018). 3X-FLAG-Ric-8A point mutant plasmids were transfected and selected for stable expression with Hygromycin B.

METHOD DETAILS

Expression and purification of myristoylated Gα_{i1} for Ric-8A complex formation

Myristoylated Gα_{i1} was expressed and purified as described previously (Mumby and Linder, 1994) with some modifications. In brief, a hexa-histidine tag was inserted between amino acid residues M119 and T120 of the wild-type human Gα_{i1}. The modified *GNAI1* gene was cloned into a pETDuet-1 vector (Sigma Aldrich) together with the *NMT1* gene that encodes for the N-myristoyl transferase from *Saccharomyces cerevisiae*. Both proteins were coexpressed in JM109 (DE3) cells (Promega) grown in Terrific Broth medium. After the cells reached an OD_{600} of 0.6, protein expression was induced by addition of 0.5 mM IPTG together with 30 μM of myristic acid.

The cells were harvested after 15 hours induction at room temperature and resuspended in lysis buffer (50 mM HEPES pH 7.5, 100 mM sodium chloride, 1 mM magnesium chloride, 50 μM GDP, 5 mM beta-mercaptoethanol, 5 mM imidazole, lysozyme, and protease inhibitors). Cells were disrupted by sonification using a 50% duty cycle, 70% power for four times 45 s. Intact cells and cell debris were subsequently removed by centrifugation and the supernatant was incubated with Ni-chelated Sepharose (GE healthcare) resin for 1.5 h at 4°C. The Ni-chelated Sepharose resin was washed multiple times in batch with lysis buffer supplemented with 20 mM imidazole and then loaded into a wide-bore glass column. The protein was eluted with lysis buffer containing 200 mM imidazole and dialyzed overnight in dialysis buffer (50 mM Tris pH 7.5, 100 mM sodium chloride, 1 mM EDTA, 2 mM dithiothreitol (DTT), 10 μM GDP). To isolate myristoylated $G\alpha_{i1}$, the dialyzed protein was further purified by hydrophobic interaction chromatography using a HiPrep 16/10 Phenyl HP column (GE Healthcare). For this purpose, 3.6 M ammonium sulfate ($(NH_4)_2SO_4$) was added dropwise to the protein to adjust the concentration to 1.2 M. Precipitated protein was removed by centrifugation and filtration and the protein was loaded onto a HiPrep 16/10 Phenyl HP column equilibrated with buffer A (50 mM Tris pH 7.5, 100 mM sodium chloride, 1 mM EDTA, 2 mM DTT, 10 μM GDP, 1.2 M $(NH_4)_2SO_4$. The column was washed with 5 column volumes of buffer A before the protein was eluted with a linear gradient 0%–100% of buffer B (50 mM Tris pH 7.5, 100 mM sodium chloride, 1 mM EDTA, 2 mM DTT, 10 μM GDP) over 45 min. The myristoylated protein was concentrated and dialyzed overnight in buffer containing 20 mM HEPES pH 7.5, 100 mM sodium chloride, 1 mM magnesium chloride, 100 μM TCEP, and 10 μM GDP. After concentrating the protein, it was flash frozen in liquid nitrogen and stored at −80°C until further use.

Formation and purification of the Ric-8A-$G\alpha_{i1}$ complex

Phosphorylated Ric-8A protein purified from insect cells was mixed with myristoylated $G\alpha_{i1}$ at a stoichiometric ratio of 1:1.5 and incubated for 90 min at room temperature. To stabilize the complex, 2.5 U of Apyrase was added to enzymatically digest GDP. After additional incubation for 90 min at room temperature, the complex was concentrated and further purified by size exclusion chromatography to remove monomeric $G\alpha_{i1}$ and Ric-8A. For this purpose, the protein was loaded on a Superdex 200 Increase 10/300 GL column equilibrated with SEC buffer (20 mM HEPES pH 7.5, 100 mM sodium chloride, 100 uM TCEP). The complex peak was collected and concentrated to 15 mg/mL for cryoEM imaging.

Expression and purification of the Ric-8A-$G\alpha_q$ complex

The glutathione S-transferase (GST) tag, followed by a tobacco etch virus (TEV) protease site, was added to the N terminus of unmodified rat Ric-8A as described (Chan et al., 2011a). This construct as well as untagged, wild-type human $G\alpha_q$ were cloned into pFastBac1 expression vectors and recombinant baculoviruses were prepared using the Bac-to-Bac baculovirus expression system (Thermo Fisher). *Trichoplusia ni* cells (Expression Systems) were co-infected with both viruses at a ratio of 1:5 (GST-TEV-Ric-8A:$G\alpha_q$) at a cell density of 3.0×10^6 cells per mL. Cultures were harvested 48 hours post infection and incubation at 27°C with gentle rotation. Cells were lysed in CHAPS buffer (20 mM HEPES pH 7.5, 100 mM sodium chloride, 1 mM DTT, 11 mM CHAPS, protease inhibitors, 1 mM magnesium chloride, and 5 U Apyrase) by Dounce homogenization followed by sonification using a 50% duty cycle, 70% power for four times 45 s. The soluble fraction was incubated with Glutathione resin (Genscript) for 1 hour at 4°C. The Glutathione resin was washed several times in batch with CHAPS buffer and then loaded into a wide-bore glass column. The complex was eluted with CHAPS buffer supplemented with 10 mM reduced glutathione and dialyzed overnight at 4°C in dialysis buffer (20 mM HEPES pH 7.5, 100 mM sodium chloride, 1 mM DTT, and 11 mM CHAPS). During dialysis, TEV protease (1:5 w/w) was added to the dialysis cassette to cleave off the amino-terminal GST-tag from Ric-8A. The cleaved GST tag and uncleaved fractions were removed by loading the protein onto Glutathione resin at 4°C. The flow through containing Ric-8A-$G\alpha_q$ complex, was concentrated and further purified by size-exclusion chromatography using a Superdex 200 Increase 10/300 column equilibrated with SEC buffer (20 mM HEPES pH 7.5, 100 mM sodium chloride, 100 uM TCEP). The monomeric complex peak was collected and re-run on a Superdex 200 Increase 10/300 GL column to remove oligomers and finally concentrated to approximately 15 mg/mL for cryoEM imaging.

Expression and purification of non-myristoylated $G\alpha_{i1}$ protein and the $G\alpha_{i1}$-ΔF354 mutant

Human $G\alpha_{i1}$ subunit and $G\alpha_{i1}$-ΔF354 with an amino-terminal 6x histidine tag followed by a rhinovirus 3C protease side were expressed in Rosetta 2 (DE3) cells (Merck) using pET21a. Cells were grown in Terrific Broth to OD_{600} of 0.6, and protein expression was induced by addition of 0.5 mM IPTG. After 15 h of incubation at room temperature, cells were harvested and resuspended in lysis buffer (50 mM HEPES pH 7.5, 100 mM sodium chloride, 1 mM magnesium chloride, 50 μM GDP, 5 mM beta-mercaptoethanol, 5 mM imidazole, lysozyme, and protease inhibitors). Cells were disrupted by sonification using a 50% duty cycle, 70% power for four times 45 s. Intact cells and cell debris were subsequently removed by centrifugation and the supernatant was incubated with Ni-chelated Sepharose (GE healthcare) resin for 1.5 h at 4°C. The Ni-chelated Sepharose resin was washed multiple times with lysis buffer in batch and then loaded into a wide-bore glass column, and protein was eluted with lysis buffer containing 200 mM imidazole. The eluted protein was dialyzed overnight in dialysis buffer (20 mM HEPES pH 7.5, 100 mM sodium chloride, 1 mM magnesium chloride, 20 μM GDP, 5 mM beta-mercaptoethanol, and 5 mM imidazole). The amino terminal histidine tag was cleaved by adding 1:1000 w/w 3C protease into the dialysis bag. Uncleaved protein, cleaved histidine tag, and 3C protease were subsequently removed by incubation with Ni-NTA resin for 45 min at 4°C. The resin was loaded into a wide-bore glass column and the flow-through containing the Gα subunit was collected. The protein was concentrated and run on a Superdex 200 10/300 GL column in SEC buffer (20 mM HEPES pH 7.5, 100 mM sodium chloride, 1 mM magnesium chloride, 20 μM GDP, and 100 uM TCEP).

Purification of His8-MBP-Ric-8A(423-530) for GDP release assay

The DNA encoding residues 423 to 530 of the C terminus of Ric-8A was cloned into a pMal vector to generate a construct containing a N-terminal octahistidine tag followed by the maltose binding protein and Ric-8A(423-530) (His8-MBP-Ric-8A(423-530)). Rosetta 2 (DE3) cells (Merck) transformed with pMal-His8-MBP-Ric-8A(423-530) were grown in Terrific Broth medium at 37°C to an OD_{600} of 1. For protein expression, the cells were induced with 0.5 mM IPTG for 15 hours at room temperature. After harvesting the cultures, cells were disrupted by sonification using a 50% duty cycle, 70% power for four times 45 s in buffer containing 50 mM HEPES pH 7.5, 100 mM sodium chloride, 5 mM beta-mercaptoethanol, 5 mM imidazole, protease inhibitors, and lysozyme. Intact cells and cell debris were subsequently removed by centrifugation and the supernatant was incubated with Ni-chelated Sepharose (GE healthcare) resin for 1.5 h at 4°C. The Ni-chelated Sepharose resin was washed 3 times in batch using wash buffer (50 mM HEPES pH 7.5, 100 mM sodium chloride, 5 mM beta-mercaptoethanol, protease inhibitors, and 20 mM imidazole). After loading the resin into a wide-bore glass column, it was washed with 10 column volumes of wash buffer before the protein was eluted in wash buffer supplemented with 200 mM imidazole. The eluted protein was concentrated and further purified by size-exclusion chromatography using a Superdex 200 Increase 10/300 GL column and SEC buffer (20 mM HEPES pH 7.5, 100 mM sodium chloride, and 100 uM TCEP) to remove oligomers and free MBP. The monomeric protein was collected, concentrated, and flash frozen in liquid nitrogen for further usage.

In vitro phosphorylation of MBP-Ric-8A (423-530)

Purified His8-MBP-Ric-8A(423-530) (4 mg) was phosphorylated with 60 μg of Casein Kinase II (CKII) (New England Biolabs Inc.) for 2 hours at 30°C in 4 mL of phosphorylation buffer (20 mM HEPES pH 7.5, 100 mM sodium chloride, 5 mM EDTA, 100 uM TCEP, 10 mM magnesium chloride, and 250 μM ATP. The phosphorylated protein was further purified by size-exclusion chromatography and phosphorylation was analyzed with Pro-Q Diamond Phosphoprotein Gel Stain (Thermo Fisher).

GDP release assay

The GDP release assay was performed with purified full-length Ric-8A or MBP-Ric-8A(423-530) protein in the unphosphorylated or phosphorylated state, respectively, and $G\alpha_{i1}$. For this purpose, $G\alpha_{i1}$ in 20 mM HEPES pH 7.5, 100 mM sodium chloride, 1 mM magnesium chloride, 100 μM TCEP, and 5 μM GDP was diluted to 0.4 μM in GDP-loading buffer (20 mM HEPES pH 7.5, 150 mM sodium chloride, 1 mM EDTA pH 8.0, 100 μM TCEP) and ^{3}H-GDP (39.8 Ci/mmol, Perkin Elmer) was added to a final concentration of 2.5 μM. After incubation for 60 min at room temperature, the GDP release was initiated upon the addition of Ric-8A proteins (0 or 1 μM) in reaction buffer (20 mM HEPES pH 7.5, 100 mM sodium chloride, 1 mM magnesium chloride, 100 μM TCEP, and 100 μM GTPγS). At 0 and 20 min, 500 uL of ice-cold wash buffer (20 mM HEPES pH 7.5, 150 mM sodium chloride, 20 mM magnesium chloride, 30 uM aluminum sulfate, 5 mM sodium fluoride) was added to 20 uL of the reaction and the mixture was immediately filtered using a microanalysis filter holder (EMD Milipore) and pre-wet mixed cellulose filters (25 mm, 0.22 μm). The filter was washed three times with 500 μL ice-cold wash buffer and dried for at least 1 h at room temperature. The amount of radioactivity that remained bound to the filters was determined by liquid scintillation spectrometry. GDP release data were analyzed using GraphPad Prism.

Fluorescence polarization spectroscopy

FITC-labeled Ric-8A (504-530) peptide with phosphoserines at positions 522, 523, and 527 was obtained by custom peptide synthesis from Tufts University Core Facility and dissolved to an approximate concentration of approximately 1mM in 100 mM HEPES pH 7.4. The exact concentration was then determined by diluting the stock appropriately to be in a linear absorbance range and by measuring the FITC absorbance at 495 nm. Using the chosen dilution factor and the calculated extinction coefficient at pH 7.5 of 84000 cm^{-1} M^{-1}, the exact stock concentrations was calculated. Fluorescence polarization spectroscopy measurements were performed and analyzed based on published guidelines (Moerke, 2009; Rossi and Taylor, 2011). To perform saturation binding experiments, two-fold dilution series in 20 mM HEPES pH 7.4, 100 mM sodium chloride, 100 μM TCEP, 0.01% (w/v) DDM and 20 μM GDP of unlabeled $G\alpha_{i1}$, $G\alpha_{s}$, and α-helical domain of $G\alpha_{i1}$ ($G\alpha_{i1}$-AHD) were made, yielding twelve samples with final concentrations ranging from 592 μM to 0.07 μM, 550 μM to 0.07 μM, and 1008 μM to 0.1 μM, respectively. Each of these samples was incubated with FITC-labeled peptide for 1 hour at room temperature prior to measurements, and for each dataset, a control sample containing no protein was included to measure the free anisotropy of FITC-labeled peptide. The FITC-labeled Ric-8A (504-530) was used at a final concentration of 4 nM in all assays. Measurements were performed in quintuplicate in a 384-well plate on a Tecan Infinite M1000 (Tecan Life Sciences), using an excitation wavelength of 470 nm, an emission wavelength of 525 nm and excitation, and emission bandwidths of 5 nm. The obtained data was fit using "One Site – Total" nonlinear regression in GraphPad Prism.

CryoEM data acquisition and processing

3.5 μl of Ric-8A-$G\alpha_{i}$ or Ric-8A-$G\alpha_{q}$ (~5mg/mL) supplemented with 0.05% (w/v) β-octyl glucoside detergent was applied to freshly glow-discharged gold holey carbon grids (Quantifoil, Au-R1.2/1.3) under 100% humidity. Excess sample was blotted away for 1.5 s at 20°C, and the grids were subsequently plunged-frozen using a Vitrobot Mark IV (Thermo Fisher Scientific).

Ric-8A-Gα protein complexes were imaged at cryogenic temperatures with a Titan Krios G2 (ThermoFisher Scientific) transmission electron microscope with a post column energy filter (20mV slit width) operated at 300 kV on a Gatan K2 Summit direct electron camera at a magnification of × 130,000 (1.06 Å/pixel) for Ric-8A-$G\alpha_{i1}$ and × 165,000 (0.82 Å/pixel) for Ric-8A-$G\alpha_{q}$. 3095 micrographs,

dose fractioned over 50 frames, for Ric-8A-Gα_{i1}, and 7560 micrographs, dose fractioned over 48 frames, for Ric-8A-Gα_q complexes, were recorded with a dose rate of 1.3 e/Å2 (7.3 e/pixel/second) using counted mode with a defocus range of 1.0–2.0 μm using SerialEM (Mastronarde, 2005). Beam induced anisotropic image motion on the micrographs was corrected using MotionCor2 (versions; 1.2.1 and 1.2.6) (Zheng et al., 2017) with dose weighting. Contrast transfer function values of each micrograph was initially determined using both CtfFind4 (Rohou and Grigorieff, 2015) and Gctf 1.06 (Zhang, 2016) and further refined using Relion3 (Zivanov et al., 2018). Auto-picked particle projections, 4,723,551 for Ric-8A-Gα_q and 4,960,082 for Ric-8A-Gα_{i1}, were subjected to several rounds of two-dimensional reference-free alignment to exclude damaged particles and contaminations using Relion3 (Zivanov et al., 2018). The initial models for both maps were obtained using Relion3 stochastic gradient descent algorithm implemented from cryoSPARC (Punjani et al., 2017). The particles in the well-defined 2D classes were further processed with several rounds of 3D classification to remove particles populating poorly defined classes. Initial 3D classifications yielded 424,000 high quality particle projections for Ric-8A-Gα_q and 727,000 for Ric-8A-Gα_{i1}. The core part of both Ric-8A-Gα complexes were stable across several 3D classifications, in contrast to the C-terminal extended region of Ric-8A that displayed variability. The most complete maps were obtained by selection of particle sets belonging to classes with clear density around the C-terminal extended loop of Ric-8A. Around 70,000 and 153,000 particles for Ric-8A-Gα_q and Ric-8A-Gα_{i1}, respectively, were refined independently to obtain maps with global indicated resolution of 3.5 and 4.1 Å, respectively, using the FSC 0.143 criterion. The masks used for final refinements were generated with Relion3 and excluded the α-helical domain. Local resolution maps were generated with Relion3.1. Validation of cryoEM maps and models was performed with PHENIX (Liebschner et al., 2019). Three-dimensional orientation distribution is assessed by 3D-FSC curves generated using the 3DFSC tool (Tan et al., 2017). UCSF Chimera was used for map/model visualizations and figure preparation (Pettersen et al., 2004).

Model building and refinement

Initial models of Ric-8A-Gα_{i1} and Ric-8A-Gα_q were built by rigid-body fitting of the Ric-8A (residues 1-423) (PDB: 6NMG) (Zeng et al., 2019), as well as the Ras-like domain of Gα_{i1} (PDB: 1GP2) (Wall et al., 1995) and Gα_q (PDB: 3AH8) (Nishimura et al., 2010) into the cryoEM maps. Ric-8A residues 424-482 of the Ric-8A-Gα_{i1} and 424-484 of the Ric-8A-Gα_q complex, as well as the β6-α5 loop and α5 helix of Gα_{i1} and Gα_q, were built by *de novo* modeling. For most of Ric-8A, the map quality was sufficient for building and assign side chains, except for the C-terminal residues 452-484 in the Ric-8A-Gα_q complex that did not allow unambiguous assignment of the registration of amino acid residues. As a result, residues 452-457 were not included in the final model and residues 458-484 were built as a poly alanine model. The map quality in this region was better in the Ric-8A-Gα_{i1} structure and allowed building of the Ric-8A model up to residue 482 including side chains. The Ras-like domain of Gα_{i1} was modeled between residues 32-54 and 193-354 due to the poor density of the alpha helical domain (residues 63−176) and adjacent loops that was only visible in low-pass filtered maps. For Gα_q, we were only able to build a model for residues 217-359 due to the weaker cryoEM map density in the N-terminal region compared to Gα_{i1}. Side chains and loop residues without sufficient EM density were stubbed or completely deleted.

The starting models were then subjected to iterative rounds of manual refinement in Coot (Emsley et al., 2010) and real space refinement in Phenix (Adams et al., 2011). The final models were visually inspected for general fit to the maps and the geometry was analyzed using MolProbity (Williams et al., 2018) as part of the Phenix software suite. The final refinement statistics for both models are summarized in supplemental data (Table S1). All molecular graphics figures were prepared with UCSF Chimera (Pettersen et al., 2004). Residue numbering for the interaction profiles between Ric-8A and Gα subunits (Figure S7) are based on Gα_{i1} and the ''common Gα numbering (CGN) system in superscript'' (Flock et al., 2015).

Generation of a homology model of Ric-8B-Gα_s

A homology model of the Ric-8B-Gα_s complex was generated by using SWISS-MODEL (Waterhouse et al., 2018). For this purpose, we used the Ric-8A-Gα_q structure as a template, including Ric-8A residues 1-451 and the poly-alanine model of the C-terminal tail (residues 458- 484) as well as Gα_q 217-359. For the target sequences we used the Uniprot entries P63092 (human Gα_s) and Q9NVN3 (human Ric-8B).

Protein Thermal Stability Assays

Thermal stability of indicated Ric-8A proteins were analyzed by a SYPRO Orange fluorescent dye-based denaturation assay using a Bio-Rad C1000 – CFX96 Real-Time PCR detection system. SYPRO Orange dye was added at 1000x dilution in samples containing 0.5mg/mL Ric-8A 1-452 or full-length with or without phosphorylation (Buffer: 20 mM HEPES pH:7.4, 140 mM KCl, 5% glycerol and 1mM TCEP). Fluorescence of SYPRO orange is measured between 10 to 80°C (30 s per 1°C increments) using the SYBR channel on the CFX96 plate reader.

Cell culture and cell line generation

Wild-type and *RIC-8A* knockout HEK293T cell lines were cultured in DMEM with 10% (v/v) FBS. The *RIC-8A* knockout cell line was generated using CRISPR technology (Papasergi-Scott et al., 2018) *RIC-8A* knockout cell lines with stably-expressed 3X FLAG-tagged Ric-8A point mutants were generated by transfection of pcDNA3.1-Hygro-3XFlag-TEV-Ric-8A point mutant plasmids and selection with 300 μg/mL Hygromycin B.

Membrane preparation and Immunoblotting

Cells were washed and harvested in PBS containing protease inhibitor cocktail (23 μg/mL phenylmethylsulfonyl fluoride, 21 μg/mL Na-*p*-tosyl-L-lysine-chloromethyl ketone, 21 μg/mL L-1-*p*-tosylamino-2-phenylethyl-chloromethyl ketone, 3.3 μg/mL leupeptin, and 3.3 μg/mL lima bean trypsin inhibitor). Cells were suspended in 20 mM HEPES, pH 8.0, 150 mM NaCl, 2 mM $MgCl_2$ and 1 mM EDTA, and protease inhibitor cocktail and lysed using a nitrogen cavitation device (Parr Industries). The lysates were centrifuged at 750 g and the supernatants were centrifuged at 100,000 g for 30 min. The pelleted membranes were suspended in 2X SDS sample buffer. The amido black protein assay was used to quantify total protein in all samples (Schaffner and Weissmann, 1973). The lysates were resolved by 12% SDS-PAGE, transferred to nitrocellulose and immunoblotted with a Gq/11α antibody (Millipore 06-709).

Multiple sequence alignment and secondary structure prediction

The multiple sequence alignment for Ric-8 was done using Clustal Omega program (Madeira et al., 2019) and displayed using Jalview software (Waterhouse et al., 2009). The following species and their corresponding reference sequences are used for the *RIC-8* multiple sequence alignment*;* Ric-8A *Rattus norvegicus* (NP_001093990.1), Ric-8A *Homo sapiens* (NP_001273063.1), Ric-8B *Homo sapiens* (NP_001317074.1), Ric-8 *Drosophila melanogaster* (NP_001285048.1), Ric-8 *Caenorhabditis elegans* (NP_001023561.1) and Ric-8 *Xenopus tropicalis* (NP_989159.1).

The secondary prediction for Ric-8A was done using PSIPRED 4.0 (Jones, 1999), visualized by Jalview (Waterhouse et al., 2009) and the previously known phosphorylation sites are manually added to its corresponding figure.

QUANTIFICATION AND STATISTICAL ANALYSIS

GDP dissociation was quantified by liquid scintillation spectrometry using a scintillation counter (Beckman). The counts after 20 min incubation time were normalized to the counts at time point zero to calculate the percentage of bound GDP: (counts at t_{20}): (counts at t_0). Experiments were run at least in triplicate and error bars are the mean ± SD.

Western blot band intensities were quantified by pixel densitometry analysis using Adobe Photoshop. Images were inverted and band intensities were measured using the formula: (Mean pixel intensity * area) - (Mean pixel intensity blank * area). Western blots were run in triplicate and error bars are the mean ± SEM.

DATA AND CODE AVAILABILITY

The atomic coordinates of the Ric-8A-Gα_q and Ric-8A-Gα_{i1} have been deposited in the Protein Data Bank (PDB) under accession number PDB: 6VU5 and PDB: 6VU8, respectively. The cryoEM maps of Ric-8A-Gα_q and Ric-8A-Gα_{i1} have been deposited in the Electron Microscopy Data Bank (EMDB) with the codes EMDB: EMD-21387 and EMDB: EMD-21388, respectively.

Cell Reports, Volume *30*

Supplemental Information

Structures of Gα Proteins in Complex with Their Chaperone Reveal Quality Control Mechanisms

Alpay Burak Seven, Daniel Hilger, Makaía M. Papasergi-Scott, Li Zhang, Qianhui Qu, Brian K. Kobilka, Gregory G. Tall, and Georgios Skiniotis

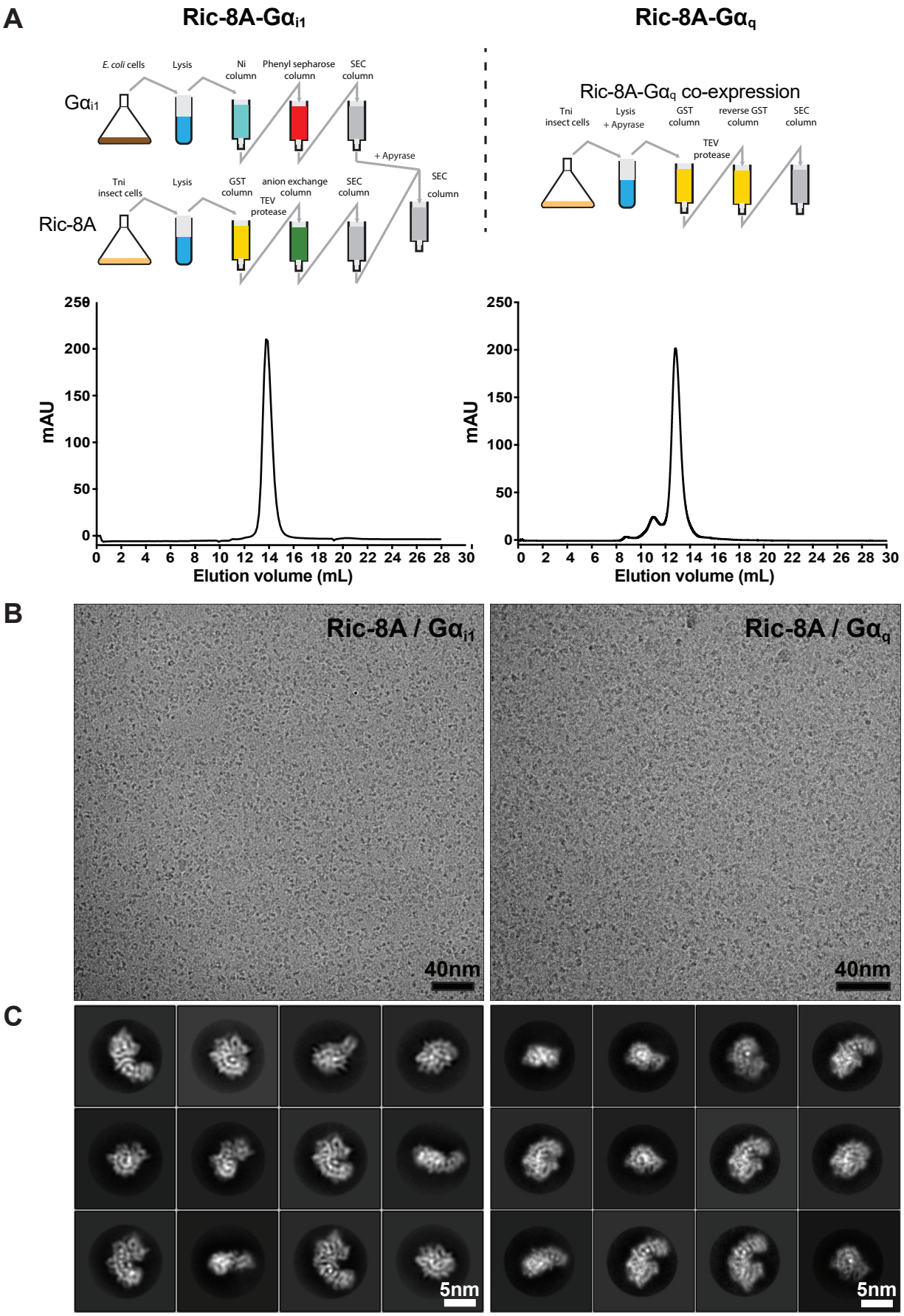

Supplementary Figure 1. Overview of protein purification strategies and cryoEM imaging. (A) Representative elution profile of purified Ric-8A-Gα_{i1} and Ric-8A-Gα_q complexes on Superdex200 Increase 10/300 size-exclusion column. (B) Representative cryoEM micrographs and (C) 2D class averages of full-length Ric-8A bound to full-length Gα_{i1} (left panels) and Gα_q (right panels) for ~200,000 total particle projections with each class representing between 500 to 2500 particle projections. Related to Figure 1.

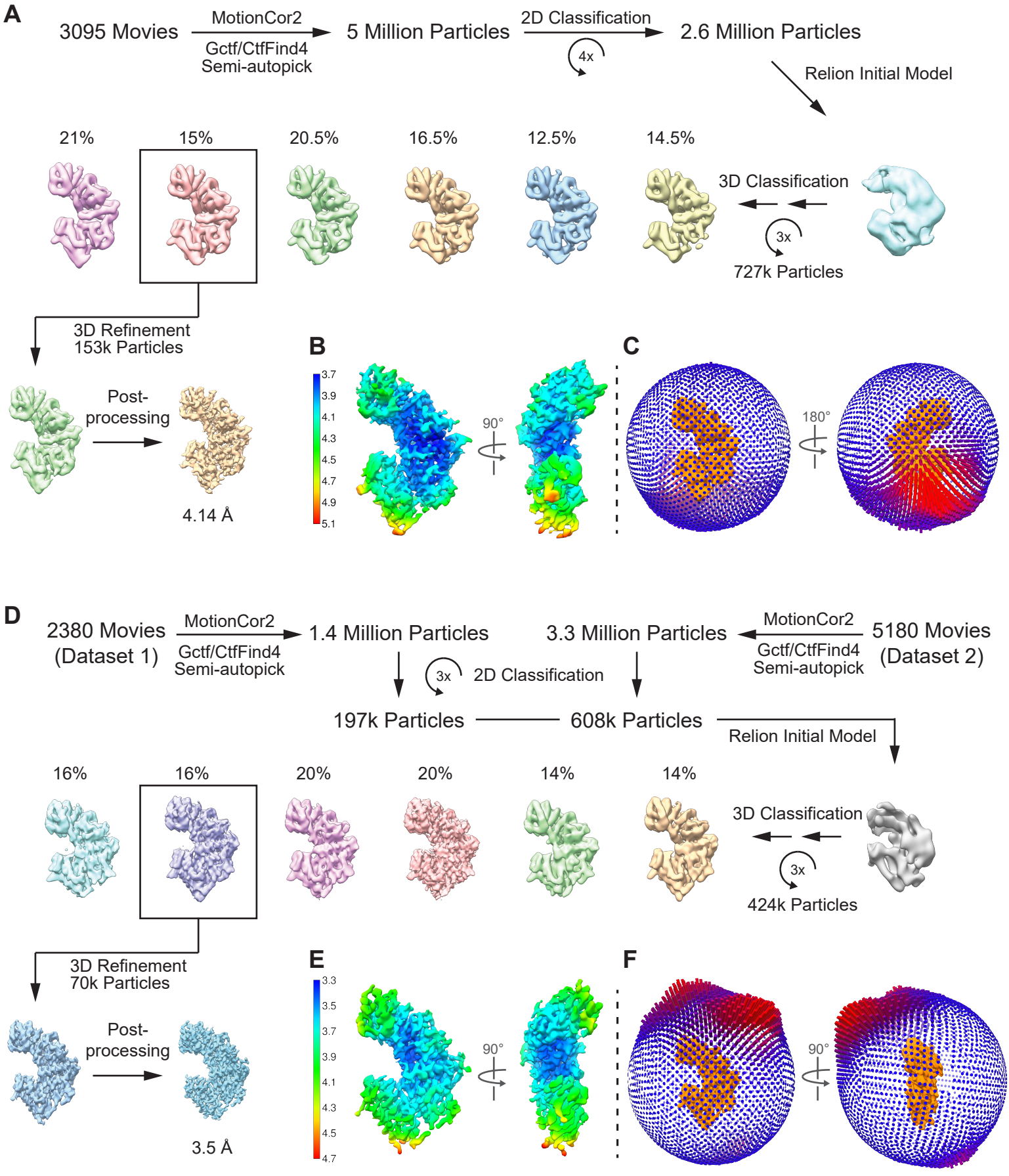

Supplementary Figure 2. CryoEM workflow for the Ric-8A-Gα complexes. (A) CryoEM processing flow-chart, (B) local resolution estimation and (C) angular distribution of the projections contributing to the refined cryoEM map of the Ric-8A-Gα_{i1} complex. (D) CryoEM processing flow-chart, (E) local resolution estimation and (F) angular distribution of the projections contributing to the refined cryoEM map of the Ric-8A-Gα_{q} complex. Related to Figure 1.

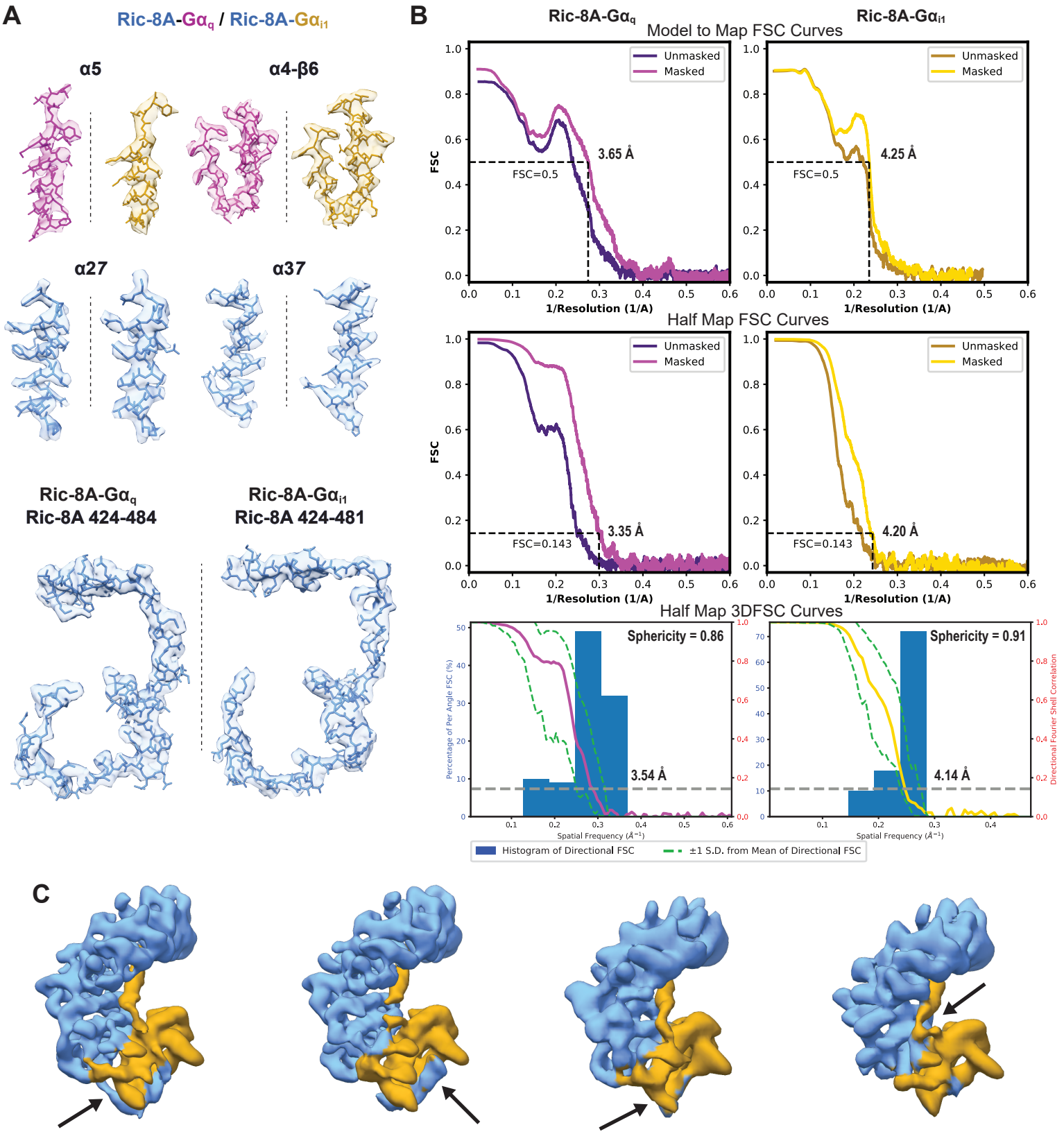

Supplementary Figure 3. CryoEM map quality and validation. (A) Representative cryoEM densities of $G\alpha_q$ (magenta) and $G\alpha_{i1}$ (gold) bound to Ric-8A (blue - left panels for $G\alpha_q$ and right panels for $G\alpha_{i1}$). (B) Fourier shell correlation plots between the model and full map and between the half maps generated using Mtriage in PHENIX and 3DFSC. Dashed lines represent the resolution values at 0.143 FSC for half maps and 0.5 FSC for the model to full map. (D) Structural variability in Ric-8A-Gα complexes. Ric-8A-$G\alpha_{i1}$ particles were subjected to iterative 3D classification rounds followed by refinement to elucidate variation across reconstructions. Corresponding Ric-8A and $G\alpha_{i1}$ densities are colored blue and gold respectively. Four representative classes are shown to highlight the structural variability (indicated by arrows) of the extended C-terminal loop region of Ric-8A, the C-terminal helix of Ric-8A interacting with the switch2 motif of $G\alpha_{i1}$, the Ras-like domain secondary structure elements that interact with guanine nucleotide and the AHD, and the loop between α5 and β6 of $G\alpha_{i1}$ including the TCAT motif respectively. Related to Figure 1.

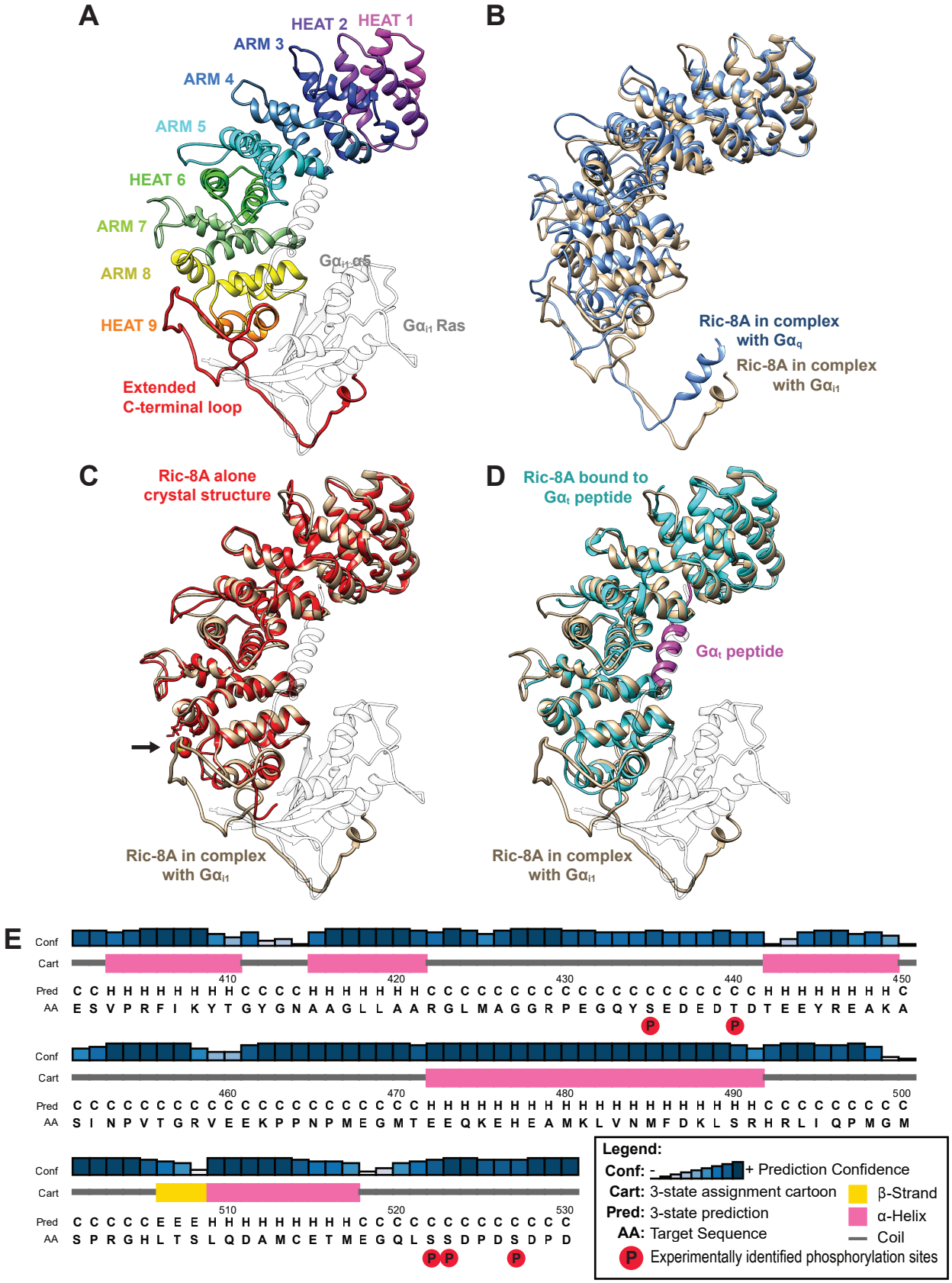

Supplementary Figure 4. Comparison of Ric-8A structures and topology of the C-terminal tail of Ric-8A. (A) Domain architecture of Ric-8A, color coded by ARM/HEAT repeats and the extended C-terminal loop, in complex with $G\alpha_{i1}$ (grey). (B) Comparison of the Ric-8A structures bound to $G\alpha_{i1}$ (tan) and $G\alpha_q$ (blue), aligned according to the first two HEAT repeats of Ric-8A to show the more compact conformation of the core ARM/HEAT repeats of Ric-8A bound to $G\alpha_q$. (C) Ric-8A-$G\alpha_{i1}$ complex structure (tan/grey) compared with the crystal structure of Ric-8A 1-453 alone (red, PDB: 6NMG); the arrow indicates the sulfate ion bound to Ric-8A in the crystal structure. (D) Ric-8A-$G\alpha_{i1}$ complex structure (tan/grey) compared with the crystal structure of Ric-8A (cyan) bound to a Gα transducin ($G\alpha_t$) peptide (purple), (PDB:6N85). (E) Secondary structure prediction of Ric-8A residues 401-530 and experimentaly identified phosphorylation sites. Related to Figure 3.

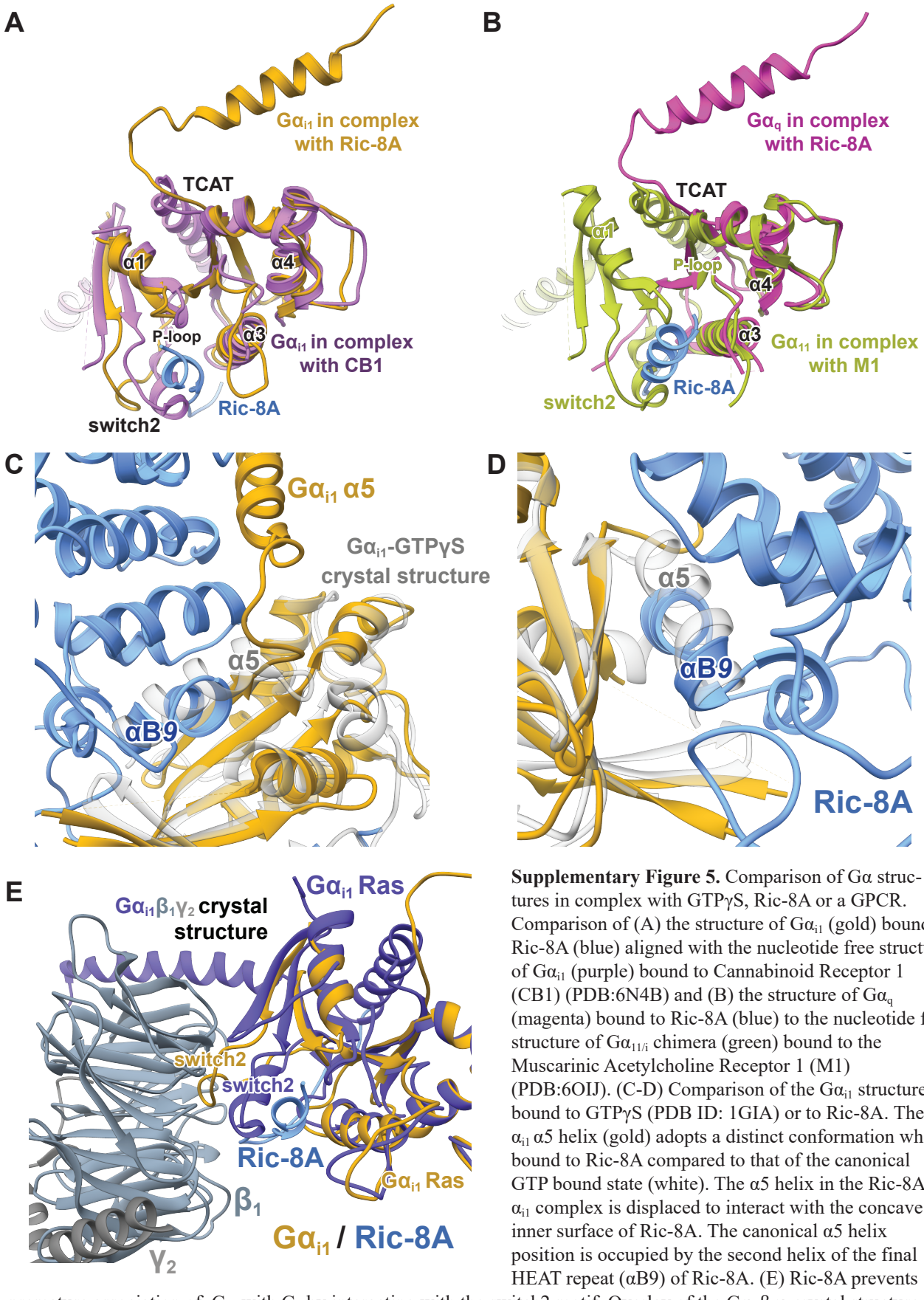

Supplementary Figure 5. Comparison of Gα structures in complex with GTPγS, Ric-8A or a GPCR. Comparison of (A) the structure of $G\alpha_{i1}$ (gold) bound to Ric-8A (blue) aligned with the nucleotide free structure of $G\alpha_{i1}$ (purple) bound to Cannabinoid Receptor 1 (CB1) (PDB:6N4B) and (B) the structure of $G\alpha_{q}$ (magenta) bound to Ric-8A (blue) to the nucleotide free structure of $G\alpha_{11/i}$ chimera (green) bound to the Muscarinic Acetylcholine Receptor 1 (M1) (PDB:6OIJ). (C-D) Comparison of the $G\alpha_{i1}$ structure bound to GTPγS (PDB ID: 1GIA) or to Ric-8A. The G α_{i1} α5 helix (gold) adopts a distinct conformation when bound to Ric-8A compared to that of the canonical GTP bound state (white). The α5 helix in the Ric-8A-G α_{i1} complex is displaced to interact with the concave inner surface of Ric-8A. The canonical α5 helix position is occupied by the second helix of the final HEAT repeat (αB9) of Ric-8A. (E) Ric-8A prevents premature association of $G_{\beta\gamma}$ with G_{α} by interacting with the switch2 motif. Overlay of the $G\alpha_{i1}\beta_1\gamma_2$ crystal structure (PDB ID:1GP2) with the cryoEM model of $G\alpha_{i1}$ (gold) bound to Ric-8A (blue). The switch2 motif interacts with Ric-8A in both $G\alpha_{i1}$ and $G\alpha_{q}$. The switch2 motif of $G\alpha_{i1}$ bound to Ric-8A adopts a different conformation than switch2 motif in either $G\alpha_{i1}$ in complex with $\beta_1\gamma_2$ (slate grey/grey) or $G\alpha_{i1}$ alone. The conformation of Gα switch2 in Ric-8A-Gα structures does not appear to be compatible with canonical $\beta_1\gamma_2$ interaction. Related to Figure 3.

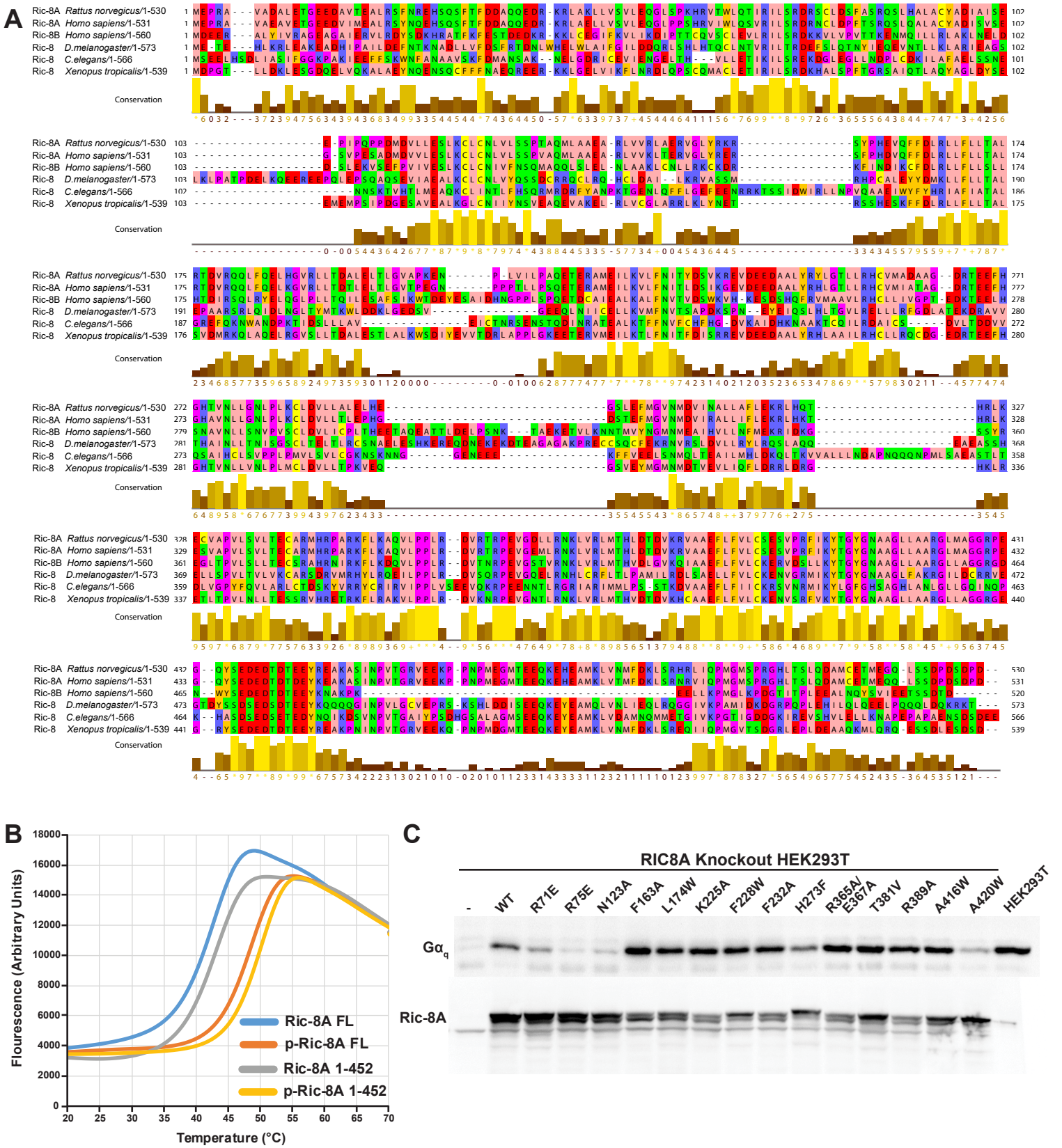

Supplementary Figure 6. Multiple sequence alignment of Ric-8, thermal stability of Ric-8A and expression control of Ric-8A mutants in the cell based Ric-8A complementation assay. (A) The sequence alignment of Ric-8 includes Ric-8A *Rattus norvegicus* (NP_001093990.1), Ric-8A *Homo sapiens*, (NP_001273063.1), Ric-8B *Homo sapiens* (NP_001317074.1), Ric-8 *Drosophila melanogaster* (NP_001285048.1), Ric-8 *Caenorhabditis elegans* (NP_001023561.1) and RIC-8 *Xenopus tropicalis* (NP_989159.1). (B) Thermal stability of full-length Ric-8A (Ric-8A FL), phosphorylated/full-length Ric-8A (p-Ric-8A FL) and truncated Ric-8A (Ric-8A 1-452), and phosphorylated/truncated Ric-8A (p-Ric-8A 1-452). The stability was analyzed using SYPRO Orange fluorescence over increasing temperatures. (C) Knockout of RIC-8A in HEK293T cells results in a $G\alpha_q$ abundance defect (Papasergi-Scott et al., 2018). The rescue of $G\alpha_q$ abundance upon stable expression of Ric-8A mutants was analyzed by quantitative immunoblotting of cell membrane samples. Representative western blot of membrane-bound $G\alpha_q$ is shown in upper panel and Ric-8A in lower panel. Related to Figure 4 and 6.

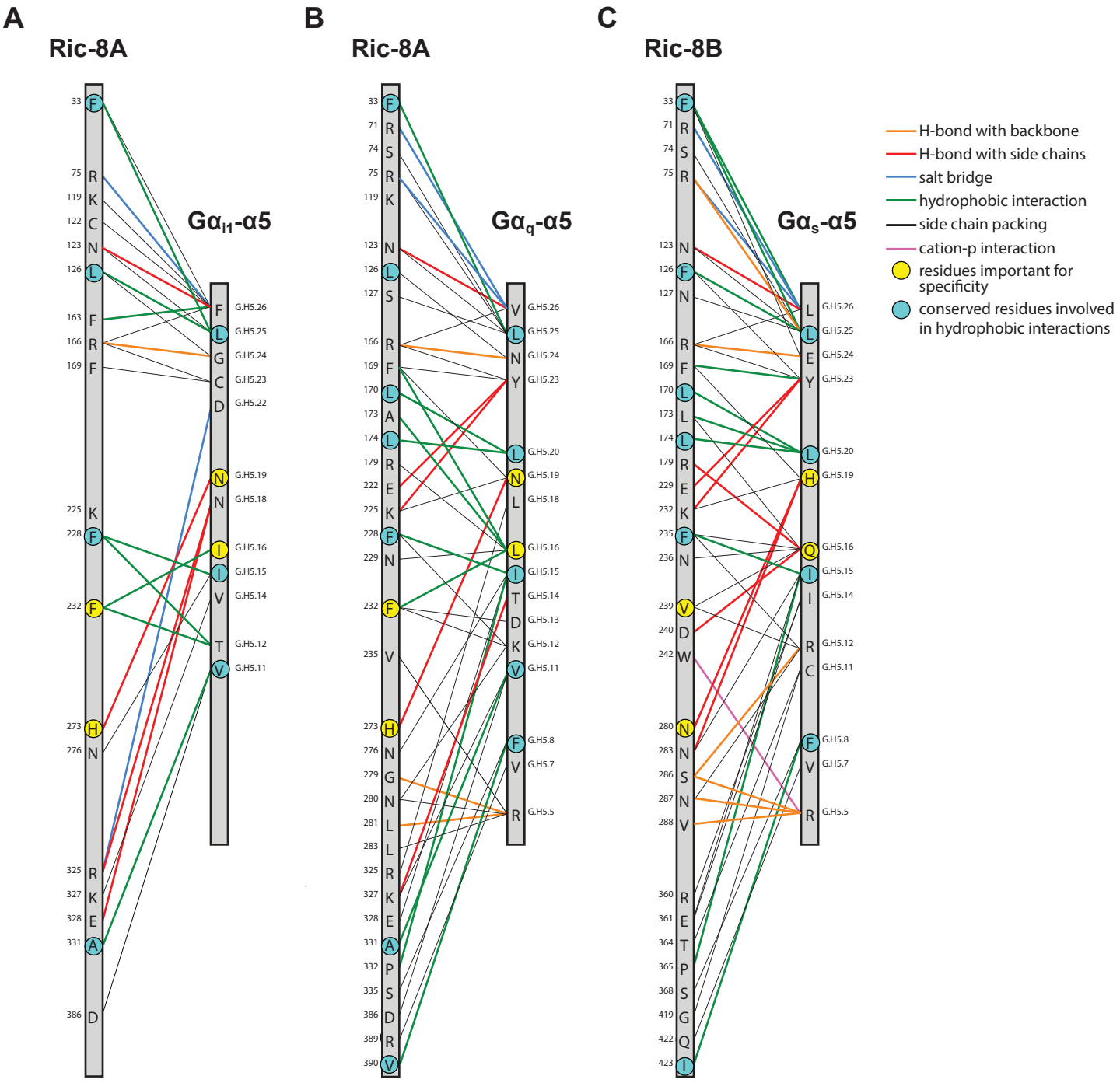

Supplementary Figure 7. Comparison of interaction profiles of the α5 helices with the Ric-8 core domain. Interaction profile of the α5 helix of (A) $G\alpha_{i1}$ or (B) $G\alpha_q$ with Ric-8A identified in the cryoEM structures, and the α5 helix of $G\alpha_s$ with Ric-8B predicted by homology modeling. Residue numbering is based on the "common Gα numbering (CGN) system in superscript" (Flock et al., 2015). Related to Figure 5.

Table S1. CryoEM data collection, refinement and validation statistics. Related to Figure 1.

Data collection and processing	**Ric-8A-Gα$_q$**	**Ric-8A-Gα$_{i1}$**
Magnification	165,000	130,000
Voltage (kV)	300	300
Electron exposure (e$^-$/Å^2)	62	65
Defocus range (μm)	1.0-2.0	1.0-2.0
Pixel size (Å)	0.82	1.06
Symmetry imposed	C1	C1
No. Initial particle images	4,723,551	4,960,082
No. Final particle images	70,439	153,110
Map resolution (Å)	3.5	4.0
FSC threshold	0.143	0.143
Map resolution range (Å)	3.2 – 4.2	3.8-4.5
Map sharpening *B* factor (Å^2)	-90	-180
Refinement		
Initial model used (PDB code)	6NMG (Ric-8A)/3AH8 (Gα$_q$)	6NMG (Ric-8A)/1GP2 (Gα$_{i1}$)
Supplied resolution (Å)	3.5	4.0
FSC threshold	0.5	0.5
Model composition		
Chains	2	2
Non-hydrogen atoms	4,657	5249
Protein residues	603	669
B factors (Å^2)	71.51	142.16
R.m.s. deviations		
Bond lengths (Å)	0.006	0.005
Bond angles (°)	0.934	1.023
Validation		
MolProbity score	1.98	1.97
Clashscore	8.28	7.78
Poor rotamers (%)	0.00	0.00
Ramachandran plot		
Favored (%)	90.53	90.08
Allowed (%)	9.47	9.92
Disallowed (%)	0	0

Table S2. Oligonucleotides. Related to Key Resources Table.

REAGENT or RESOURCE	SOURCE	IDENTIFIER
Oligonucleotides		
$G\alpha_{i1}$-ΔF354_Fw: 5'-AAAGATTGTGGTCTCTAAGC TTCTGAGATCCGGCTGC-3'	Stanford Pan Facility	Custom synthesis
$G\alpha_{i1}$-ΔF354_Rev: 5'-TCTCAGAAGCTTAGAGACCACA ATCTTTTAGATTATTTTTTATGATGACATCTGTTAC-3'	Stanford Pan Facility	Custom synthesis
Quickchange PCR forward primer for R75E: 5'-CCGAATCCTATCCGAAGACCGCAGCTGCC-3'	IDT	Customer synthesis
Quickchange PCR reverse primer for R75E: 5'-GGCAGCTGCGGTCTTCGGATAGGATTCGG-3'	IDT	Customer synthesis
Quickchange PCR forward primer for N123A: 5'-CAAATGCCTGTGTGCTCTTGTGCTCAGCAG-3'	IDT	Customer synthesis
Quickchange PCR reverse primer for N123A: 5'-CTGCTGAGCACAAGAGCACACAGGCATTTG-3'	IDT	Customer synthesis
Quickchange PCR forward primer for F163A: 5'-CGAAGTCCAGTTCGCTGACTTAAGGCTCC-3'	IDT	Customer synthesis
Quickchange PCR reverse primer for F163A: 5'-GGAGCCTTAAGTCAGCGAACTGGACTTCG-3'	IDT	Customer synthesis
Quickchange PCR forward primer for L174W: 5'-CCTGCTAACAGCCTGGCGCACTGATGTGC-3'	IDT	Customer synthesis
Quickchange PCR reverse primer for L174W: 5'-GCACATCAGTGCGCCAGGCTGTTAGCAGG-3'	IDT	Customer synthesis
Quickchange PCR forward primer for K225A: 5'-CATGGAAATCCTCGCAGTGCTCTTTAACATC-3'	IDT	Customer synthesis
Quickchange PCR reverse primer for K225A: 5'-GATGTTAAAGAGCACTGCGAGGATTTCCATG -3'	IDT	Customer synthesis
Quickchange PCR forward primer for F228W: 5'-CCTCAAAGTGCTCTGGAACATCACCTACG-3'	IDT	Customer synthesis
Quickchange PCR reverse primer for F228W: 5'-CGTAGGTGATGTTCCAGAGCACTTTGAGG -3'	IDT	Customer synthesis
Quickchange PCR forward primer for F232A: 5'-CTTTAACATCACCGCCGACTCTGTTAAGAG-3'	IDT	Customer synthesis
Quickchange PCR reverse primer for F232A: 5'-CTCTTAACAGAGTCGGCGGTGATGTTAAAG -3'	IDT	Customer synthesis
Quickchange PCR forward primer for H273F: 5'-GGAGTTCCATGGCTTCACCGTGAATCTCC-3'	IDT	Customer synthesis
Quickchange PCR reverse primer for H273F: 5'-GGAGATTCACGGTGAAGCCATGGAACTCC -3'	IDT	Customer synthesis
Quickchange PCR forward primer for R365A+E367A: 5'-GGGATGTGAGGACTGCGCCTGCGGTGGGGGACCT GCTC-3'	IDT	Customer synthesis
Quickchange PCR reverse primer for R365A+E367A: 5'-GAGCAGGTCCCCCACCGCAGGCGCAGTCCTCACAT CCC -3'	IDT	Customer synthesis
Quickchange PCR forward primer for T381V: 5'-CTTGTCCGCCTCATGGTACACCTGGATACAG-3'	IDT	Customer synthesis
Quickchange PCR reverse primer for T381V: 5'-CTGTATCCAGGTGTACCATGAGGCGGACAAG -3'	IDT	Customer synthesis
Quickchange PCR forward primer for R389A: 5'-GATACAGATGTGAAGGCAGTAGCTGCTGAGTTC-3'	IDT	Customer synthesis
Quickchange PCR reverse primer for R389A: 5'-GAACTCAGCAGCTACTGCCTTCACATCTGTATC -3'	IDT	Customer synthesis

Quickchange PCR forward primer for A416W: 5'-CTACGGGAATGCTTGGGGCCTCCTGGCTG-3'	IDT	Customer synthesis
Quickchange PCR reverse primer for A416W: 5'-CAGCCAGGAGGCCCCAAGCATTCCCGTAG -3'	IDT	Customer synthesis
Quickchange PCR forward primer for A420W: 5'-CTGCTGGCCTCCTGTGGGCCAGGGGCCTCATG -3'	IDT	Customer synthesis
Quickchange PCR reverse primer for A420W: 5'-CATGAGGCCCCTGGCCCACAGGAGGCCAGCAG -3'	IDT	Customer synthesis